Analysis of Antennas on Carbon-Fibre Composite Aircraft

Parna Kazerani

A Thesis

in the Department of

Electrical and Computer Engineering

Presented in Partial Fulfillment of the Requirements

for the Degree of

Master of Applied Science

(Electrical and Computer Engineering) at

Concordia University

Montreal, Quebec, Canada

September 2012

CONCORDIA UNIVERSITY
SCHOOL OF GRADUATE STUDIES

This is to certify that the thesis prepared

By: Parna Kazerani

Entitled: Analysis of Antennas on Carbon-Fibre Composite Aircraft

and submitted in partial fulfillment of the requirements for the degree of

Master of Applied Science

Complies with the regulations of this University and meets the accepted standards with respect to originality and quality.

Signed by the final examining committee:

_____ Chair
Dr. Ferhat Khendek

_____ Examiner, External
Dr. Rolf Wüthrich To the Program

_____ Examiner
Dr. Christopher W. Trueman

_____ Supervisor
Dr. Robert Paknys

_____ Supervisor
Dr. Jean-Jacques Laurin

Approved by: _____
Dr. W. E. Lynch, Chair
Department of Electrical and Computer Engineering

_____ _____
September 10, 2012 Dr. Robin A. L. Drew
Dean, Faculty of Engineering and
Computer Science

Abstract

Analysis of Antennas on Carbon-Fibre Composite Aircraft

Parna Kazerani

Carbon-fiber composite (CFC) materials, due to their desirable mechanical and thermal properties, have been progressively replacing metallic structures in commercial aircraft. The electrical and electromagnetic properties of these materials, including their impact on antenna performance, have been the subject of research since their introduction in aeronautical applications. It has been shown that carbon-fibre composites form effective ground planes for antennas and the antenna performance at VHF and UHF frequencies is not essentially different from metal ground planes.

However, CFC materials are prone to cracking when used in aeronautical applications. Additionally, when CFC materials are used in aircraft, joints are inevitable. These joints can be between CFC panels or CFC and metal panels in partially composite aircraft. These cracks and joints alter the current density on the airframe surface. This alteration of current density impacts the antenna radiation performance.

In this thesis, the radiation of antennas on carbon-fibre composite aircraft is studied. The airframe scattering mechanism is analyzed and guidelines for developing simplified models of aircraft geometry for antenna analyses are provided. The utility of the leading numerical techniques suitable for analysis of aircraft antennas at VHF and UHF frequencies is studied and benchmark data on the computational resources

required is provided. The impact of cracks, seams and panel joints on the antenna radiation is also studied.

Acknowledgement

I offer my sincerest gratitude to my supervisors, Dr. Robert Paknys and Dr. Jean Jacques Laurin, for their kind guidance and gracious help. This work would not have been completed without them. I would like to thank my parents and my friends for their moral support and encouragement.

Support from the National Science and Engineering Research Council (NSERC) CRD Program, the Consortium de Recherche et d'Innovation en Aerospatiale au Quebec (CRIAQ) and industry partners Bombardier Aerospace and MacDonald Dettwiler and Associates Inc. is also gratefully acknowledged.

Last but not least, I would like to thank Aidin for his support and deep love.

Contents

List of Figures

List of Tables

Chapter 1

Introduction

The desirable mechanical characteristics of Carbon-Fibre Composite (CFC) materials such as their unsurpassed strength-to-weight ratio has made these materials a suitable candidate for use in weight-sensitive structures such aircraft and spacecraft.

Since the beginning of the 1980s, CFC materials have been progressively replacing metallic structures in commercial aircraft. The use of these materials in commercial airframes, initially limited to non-critical secondary structures, have been gradually extended to primary empennage, wing and fuselage structures, as shown in Fig. 1.1. The recently developed commercial aircraft, the Boeing 787 Dreamliner and Airbus A350, utilize more than 70 % composite(CFC) structures by volume and these materials will be even more prevalent in future-generation aircraft.

The electromagnetic effects of CFC materials and their impact on the functionality of aircraft electronic systems have been the subject of research since the introduction of these materials in aeronautical applications [6, 7, 8, 9]. In this thesis, the radiation of antennas mounted on CFC aircraft is investigated.

The electrical properties of CFC materials are different from those of metal (aluminum) which is conventionally used in aircraft. Unidirectional carbon fibre layers have anisotropic electrical properties, consisting of conducting graphite fibres lying

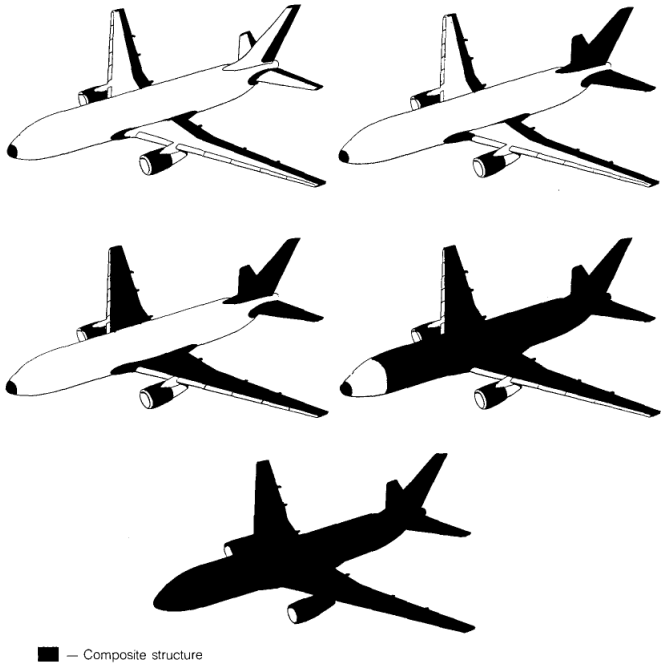

Figure 1.1: The progressive use of composites in commercial transport airframe [1].

in a dielectric material, usually epoxy resin. However, because of their weak mechanical properties normal to the fiber direction, CFC panels that are used in aircraft structures are in the form of multidirectional lay-ups of unidirectional layers or woven fabric. Experimental and theoretical works have shown that these panels simply exhibit an isotropic conductivity of $1 - 2 \times 10^4$ at VHF and UHF frequencies [8, 10]. In [11], it is shown that the performance of antennas mounted on finite conductivity ground planes for conductivities equal to 10^4 is only slightly different from the antenna performance on perfectly conducting ground planes. Thus, perfectly conducting models can be used to investigate the electromagnetic scattering properties of composite materials. This agrees well with the experimental results presented in the same paper and also in [6] and [7]. The experiments conducted in [6] and [7] show that composites form effective ground planes for antennas and the antenna performance at UHF and L band frequencies is not essentially different on metal and CFC ground planes. Thus, techniques used for analysis of antennas on metallic aircraft can be used for analysis of antennas on CFC aircraft as well.

Nevertheless, CFC materials are prone to cracking when used in aeronautical applications [1]. The matrix cracks which grow simultaneously may join each other and propagate through the matrix. Furthermore, when CFC materials are used in aircraft, joints are inevitable. These joints can be between two CFC panels or CFC and metal panels in partially composite aircraft. The impact of seams and joints in composite structures on shielding effectiveness reduction has been investigated in [6, 12], but their impact on antenna performance has not been studied.

The cracks and joints represent discontinuities which impede the current density on the airframe's surface at certain directions. This alteration of current density impacts the antenna radiation performance. At metal-CFC joints the alteration in the current density is not only the result of the discontinuities but also due to the lower conductivity of CFC compared to metal. As a matter of fact, composite possessing a conductivity 10^3 times lower than surrounding aluminum can alter the surface current distribution even with ideal joints. This can also impact the radiation performance of the antenna when located close to the junction.

Antennas are used on aircraft for manifold purposes. The radiation of an antenna is modified when mounted on an aircraft due to the scattering by the airframe. The conducting airframe forms a complex environment for which closed-form solutions do not exist. In earlier days, when the computational prediction of the performance of antennas on aircraft was not feasible, antennas were placed on aircraft through iterative trial and error experiments at some conventional locations or based on scale model measurements.

Today, advancements in computational electromagnetics and computer processing has made it feasible to predict the radiation performance of antennas on large structures such as aircraft for a range of frequencies [13, 14, 15]. Employing electromagnetic modelling tools, new antennas on new aircraft can be designed to achieve the desired radiation performance, the current location of antennas can be revisited and

mutual coupling between antennas on aircraft can be calculated prior to installation on aircraft.

Computer modelling can also be used to study the airframe scattering mechanism. In this thesis, this is accomplished by studying the interactions between the airframe and a monopole antenna mounted on the fuselage of a typical business jet. The monopole antenna simulates a blade antenna. Blade antennas are used on aircraft in Communication, Navigation and Identification (CNI) systems which require omnidirectional coverage and are essentially monopoles encapsulated in a covering to provide better aerodynamic properties [13]. The radiation of the monopole at VHF and UHF frequencies is analyzed. Modifications are made to the airframe geometry and the impact of the modifications on the antenna performance is observed to study the influence of scattering form different parts of the airframe on the antenna radiation. This study is useful for positioning antennas in the initial design stage of antenna layouts and also for developing simplified models of the aircraft geometry for antenna analysis. Simplified models of the aircraft can increase the efficiency of obtaining the solution by reducing the human effort required to create the model and also by reducing the computational cost in the case of being of smaller size than the original model. Moreover, a simplified model only consisting of certain shapes allows the possibility of employing some numerical methods that cannot be applied to the original geometry.

Other than geometry modelling, the efficiency of a numerical solution depends on the numerical technique used for treating the problem. The leading techniques for analysis of antennas on aircraft at VHF and UHF frequencies are the Multilevel Fast Multipole Method (MLFMM) [16], Physical Optics (PO) [17] and the Uniform Theory of Diffraction (UTD) [13]. PO and UTD are high frequency asymptotic techniques. The MLFMM is a computationally efficient alternative to the conventional Method of Moments (MoM). It allows full-wave analysis of antennas on electrically large

structures, such as aircraft at VHF and UHF frequencies, that cannot be solved using the classic MoM. The MoM-based electromagnetic simulation software, Feko [18], includes the parallel MLFMM technology for general 3D structures and is used in this thesis. The validity of the MoM and MLFMM for analysis of antennas on aircraft has been verified through comparison with measurements [13, 19].

In this thesis, complications involved in the above-mentioned numerical techniques are studied and numerical data on required computational resources is presented. The MLFMM is considered the most accurate technique and the validity of the two other techniques are examined through comparison with the MLFMM.

The impact of cracks, seams and panel joints on antenna radiation is also studied in this thesis. In order to basically investigate the influence of cracks and joints on the antenna radiation, simple cases of monopoles on square ground planes are analyzed. Due to the simplicity of the structure, the impact of the cracks and junctions on the antenna performance can be clearly observed.

The organization of the thesis is as follows: Chapter 2 deals with issues regarding modelling the aircraft geometry for antenna analysis. The interactions between the airframe and a quarter-wave monopole antenna mounted on a business aircraft are studied. The CAD model of the aircraft was furnished by Bombardier Aerospace [20] in a collaborative project. The radiation of the antenna on a canonical model of the aircraft, made using the simple tools available in Feko's geometry library, is also studied. Chapter 3 deals with the numerical techniques suited for analysis of antennas on aircraft at VHF and UHF frequencies, i.e., the MLFMM, PO and UTD. Chapter 4 investigates the impact of ideal CFC-metal junctions on antenna radiation. Chapter 5 studies the influence of discontinuities due to cracks and seams on the antenna radiation. The influence of cracks of different sizes and at different distances on the antenna radiation is analyzed. The radiation pattern for a monopole antenna on the aircraft when a notional crack is introduced in the airframe is also demonstrated.

Finally, conclusions are drawn in Chapter 6.

Some of the results presented in this thesis have been published in [21].

Chapter 2

Geometry Modelling

Antennas are used in airborne platforms for manifold purposes. The radiation of an antenna is modified when mounted on an aircraft. Scattering by the airframe causes the performance of an antenna mounted on aircraft to differ from the antenna performance in its conventional setting (usually on a flat ground plane or in free space).

The radiation of aircraft antennas can be examined through measurements on real aircraft or scaled models. These measurements are expensive, difficult to perform and can only determine the radiation characteristics at a limited number of frequencies and cuts. Computer modelling can be used to analyze the radiation in any desired cut and at a reduced cost.

A CAD model of the airframe is required for performing electromagnetic simulation to analyze the radiation of an antenna placed on the aircraft. Detailed modelling of a complex geometry such as an aircraft can be truly cumbersome if not impossible. The drawing tools available in EM simulation packages are not generally suited for drawing objects of great complexity. In some EM software packages such as Feko, pre-drawn objects can be imported. However, only specific file formats can be imported to the software and even with the right file formats, errors might be displayed

depending on the way the object is drawn in the drawing software. Additionally, there is often difficulty in proper meshing of the complex geometry in the EM software. The problematic mesh elements need to be fixed and this may not be easy or feasible. A meshing software can be used to mesh the aircraft drawn model so that the above problems are avoided. The mesh coordinates can then be imported to the EM software [22]. Nevertheless, there is still need for a suitable three dimensional drawing software which may be expensive and not be available to the computational electromagnetics (CEM) engineer.

The question then arises: how much would the result change if simplified models of the aircraft are used? The CAD model of the aircraft must be rigorous enough so that the accuracy of the produced results is not compromised. However, as will be seen, not all the geometrical details are necessary to obtain results within engineering accuracy. Then, how can one decide on a valid simplified model of the airframe?

This chapter addresses these questions by studying the interaction between the airframe and a monopole antenna installed on the fuselage. The fuselage forms an imperfect ground plane for the antenna and the obstructions around the antenna cause reflection and diffraction. Thus, the input impedance and radiation pattern of the monopole antenna are modified. The impact of the airframe on the above-mentioned characteristics is studied in this chapter. The study gives a good physical understanding of the airframe scattering mechanism and hence the knowledge based upon which valid simplified models of the aircraft geometry can be developed for antenna analyses. It should be noted that purposes of simplification of aircraft geometry go beyond easy drawing in the EM software. A simplified model only consisting of certain shapes allows the possibility of employing the numerical methods that cannot be applied to the original geometry. More importantly, computational efficiency can be greatly improved if the simplified model is of a smaller size than the original aircraft model. Simplified models can also be used for scaled model measurements when

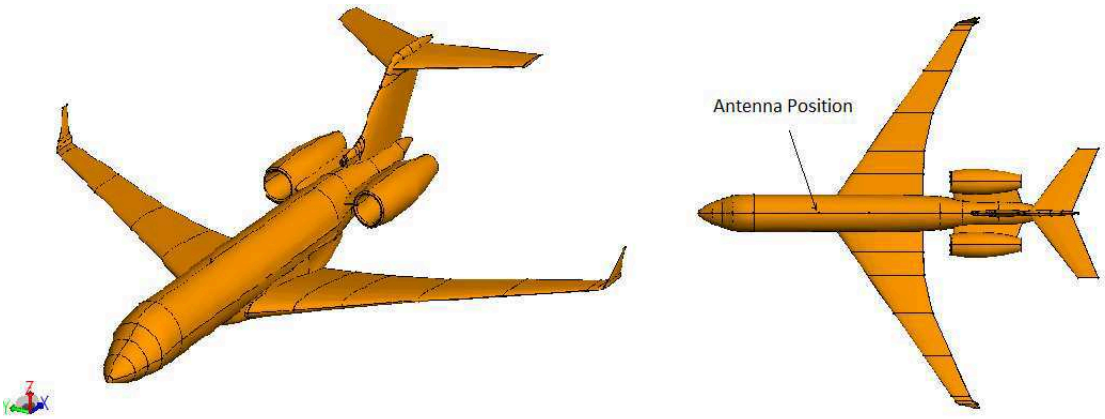

Figure 2.1: CAD model of the aircraft.

making detailed scaled models of the aircraft is difficult and time consuming.

The CAD model of a typical Bombardier business aircraft is shown in Fig. 2.1. A quarter-wave monopole is mounted on top of the fuselage forward of the wings. The aircraft is modelled as a perfect electric conductor (PEC). The aircraft has an approximate cabin radius of 1.38 meters, a cabin length of 25.85 meters and a wingspan of 27.8 meters.

The geometry was drawn in Solidworks [23] and then imported to the EM simulation software, Feko. The model was imported to Feko without much difficulties since parasolid files can be easily imported to the Feko graphical user interface, Cadfeko. A few errors occurred after the geometry was imported. Luckily, the errors could be quite easily eliminated in Feko by deleting the overlapping surfaces.

The analysis is performed at different frequencies in the VHF and UHF range. The geometry could be meshed successfully in Feko at high frequencies. At low frequencies, however, meshing creates problems. At these frequencies, the $\frac{\lambda}{10}$-size meshing of the geometry causes mesh coincident vertices along the sharp edges which lead to the singular field error on these edges. Fortunately, the problem can be fixed using the mesh fixing tools available in Feko.

The results presented in this chapter are produced using the Multilevel Fast Multipole Method (MLFMM). The validity of the MLFMM for analysis of aircraft antennas

at UHF and VHF frequencies has been verified in the literature through comparison with measurements. The results presented in this chapter are hence considered valid by "postdiction". The concept of "postdiction" formulated in [13] is that if computations obtained with a CAD model of an airframe correlates with the measurements, it is then accepted that the computations obtained with the CAD model of the modified airframe would also correlate with measurements without the need to undertake the measurements on the modified airframe.

All radiation patterns presented in this chapter are normlized gain (total) patterns.

2.1 Radiation Pattern

The radiation pattern of the monopole antenna when mounted on top of the fuselage of an aircraft is different from its radiation pattern on a flat ground plane. This is due to the cylindrical shape of the fuselage producing creeping waves as well as the obstructions around the antenna which can cause blockage, reflection and diffraction and hence affect the radiation of the antenna. Thus, the pattern of an antenna on an aircraft is affected by first order effects, i.e. line of sight (LOS) radiation and first-order reflection, as well as diffraction, creeping rays and higher order interactions. In this section, the impact of the airframe on the monopole radiation pattern is studied.

Figures 2.2 to 2.6 show the monopole radiation pattern at different VHF and UHF frequencies. The radiation pattern is studied in three principal planes, namely roll, pitch and yaw planes. The electrical size of the airframe and electrical distance of the wings, tail, nose and other parts of the airframe from the antenna depend on the frequency. Thus, by observing how the radiation pattern changes as the frequency changes, one can get some basic understanding of the airframe scattering mechanism.

It is seen that as the frequency increases, the number of ripples in the pattern increases. This is because at higher frequencies the wavelength gets smaller and

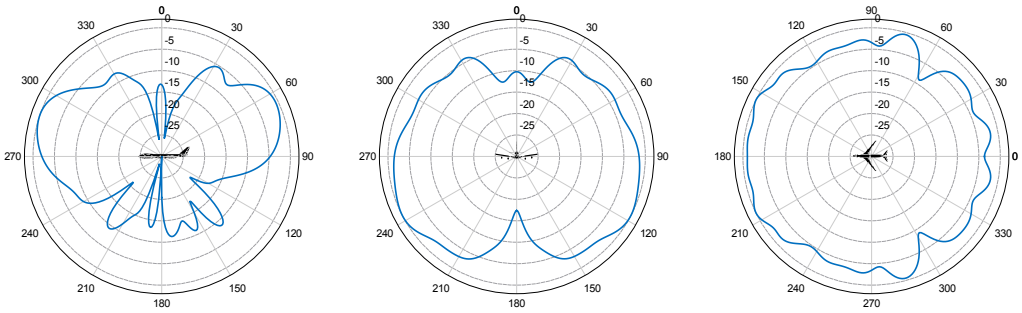

(a) (b) (c)

Figure 2.2: Radiation pattern at 50 MHz in (a) pitch plane (b) roll plane (c) yaw plane.

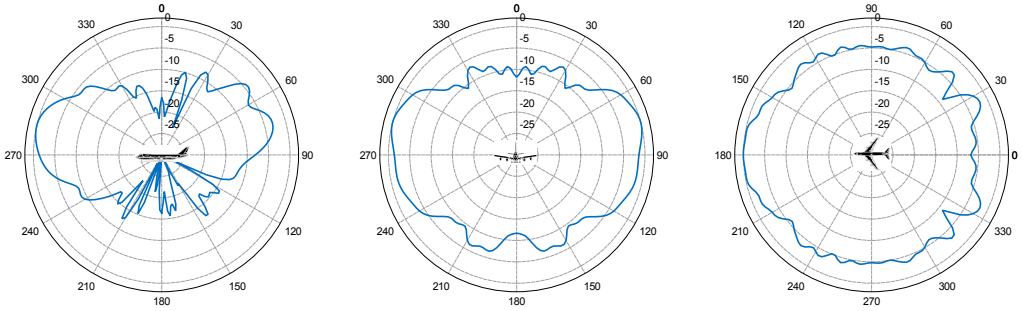

(a) (b) (c)

Figure 2.3: Radiation pattern at 100 MHz in (a) pitch plane (b) roll plane (c) yaw plane.

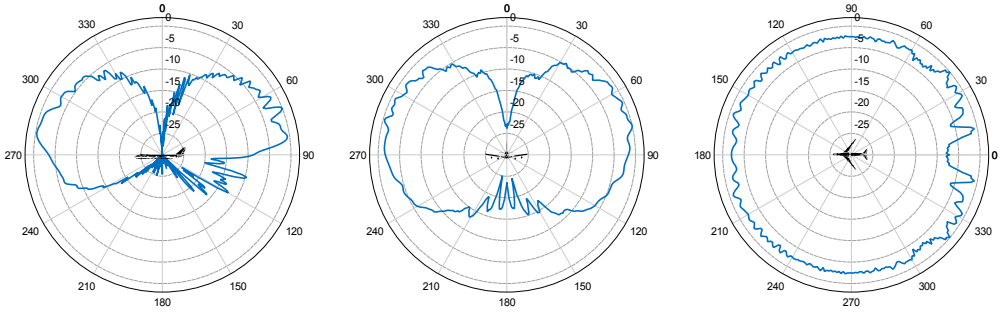

(a) (b) (c)

Figure 2.4: Radiation pattern at 500 MHz in (a) pitch plane (b) roll plane (c) yaw plane.

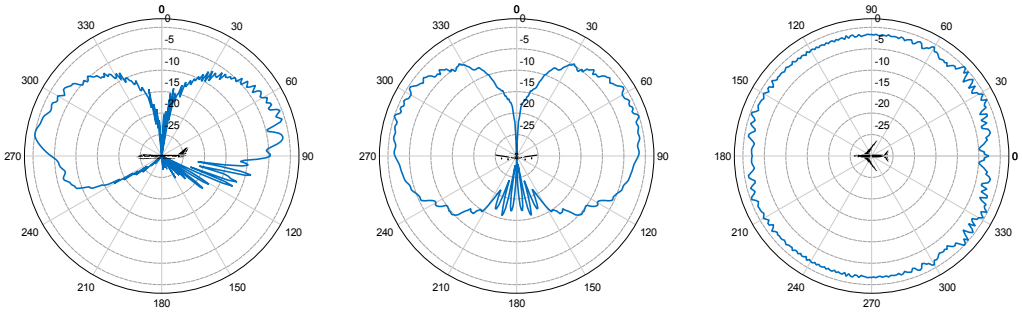

(a) (b) (c)

Figure 2.5: Radiation pattern at 700 MHz in (a) pitch plane (b) roll plane (c) yaw plane.

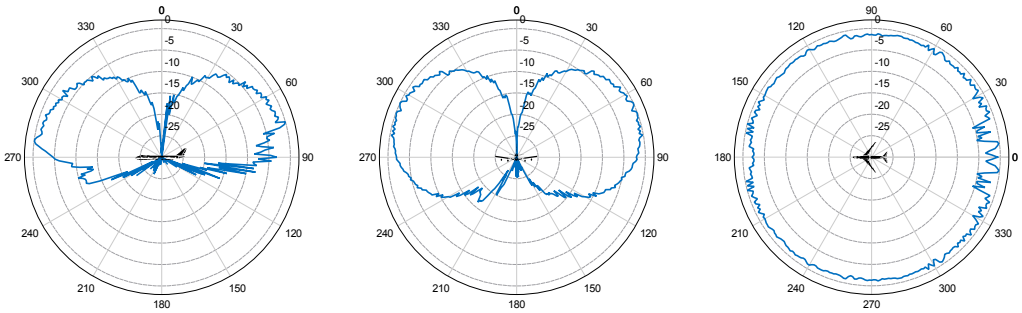

(a) (b) (c)

Figure 2.6: Radiation pattern at 2 GHz in (a) Pitch plane (b) Roll plane (c) Yaw plane.

hence there are more variations in the multipath interactions between different parts of the airframe around the aircraft.

Additionally, as the frequency increases, the radiation pattern approaches the radiation pattern of a monopole antenna located on a flat ground [24]. This was expected since at higher frequencies, the fuselage electrical diameter increases, more resembling a flat ground plane. Also, at higher frequencies the obstructions are located in a larger electrical distance from the antenna and hence interfere less with the radiation of the monopole.

At high frequencies, the roll plane pattern has a null in the zenith direction. At the lower frequencies, 100 MHz and 50 MHz, however, the behavior around the zenith direction is different. The reason for this as will be seen in section 2.1.1, is the scattering by the empennage. At low frequencies, the empennage is electrically closer to the antenna which strongly illuminates the empennage. Thus, the scattering from these parts contributes strongly in the roll plane radiation pattern and results in not having a null in the zenith. However, as the frequency increases the empennage gets electrically further away from the antenna and loses its scattering contribution to the pattern formation.

In the yaw plane, a null can be seen at the tail side at 300 MHz, 450 MHz (patterns shown in Figs. 2.9, 2.10 respectively for comparative purposes) and 500 MHz. This null is due to the LOS blockage by the empennage. At higher and lower frequencies, this null does not exist and the yaw plane pattern looks more or less isotropic. At higher frequencies, this can be explained by the fact that the empennage is electrically far from the antenna and hence its impact is hardly noticeable on the radiation pattern. At the lower frequencies, it was verified that the empennage LOS blockage is compensated for by the effective scattering from the engines that are electrically close to the antenna. Thus, the null disappears at lower frequencies and the yaw plane pattern looks more or less isotropic.

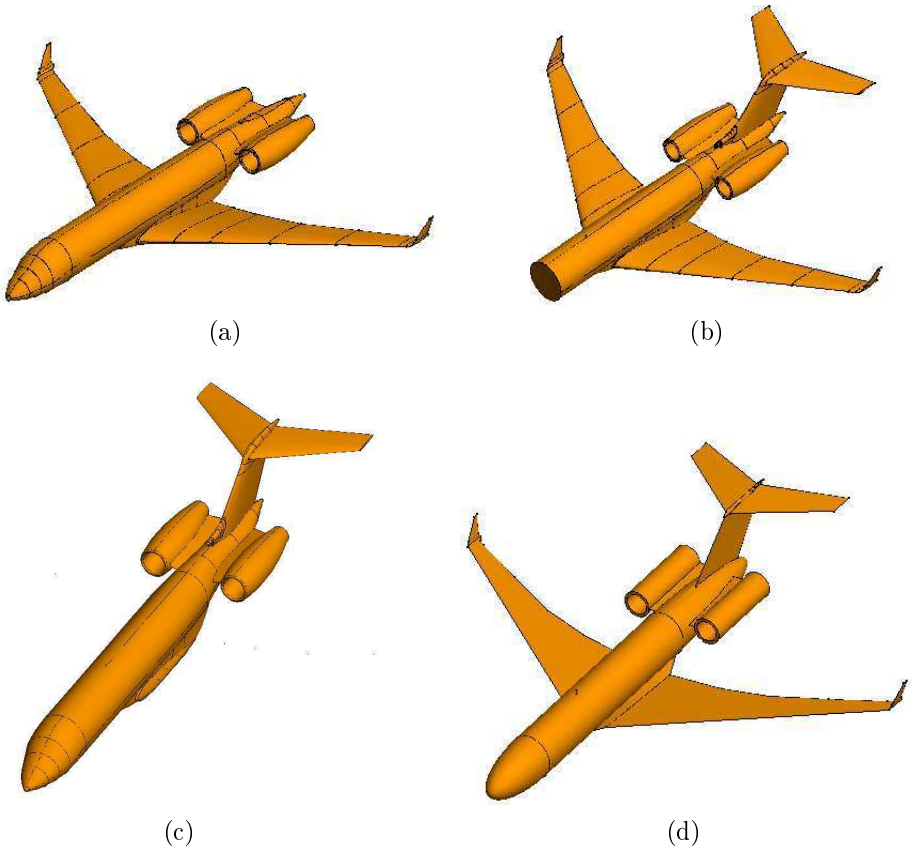

Figure 2.7: Modified aircraft models. (a) Tail-removed model. (b) Noise-removed model. (c) Wings-removed model. (d) Canonical model.

In the following sections, the effect of some geometry modifications on the radiation pattern is explored. Parts are removed from the aircraft geometry and the impact on the antenna radiation is analyzed and interpreted. The accuracy of a canonical model of the aircraft is also investigated. This approach provides a good insight to the scattering interactions between parts of the airframe and the antenna.

Alternatively, one could change the position of the monopole on top of the fuselage and observe the impact on the radiation pattern to investigate the airframe scattering [13]. By changing the position, the distance of airframe obstructions from the antenna and hence their contribution to the antenna radiation varies.

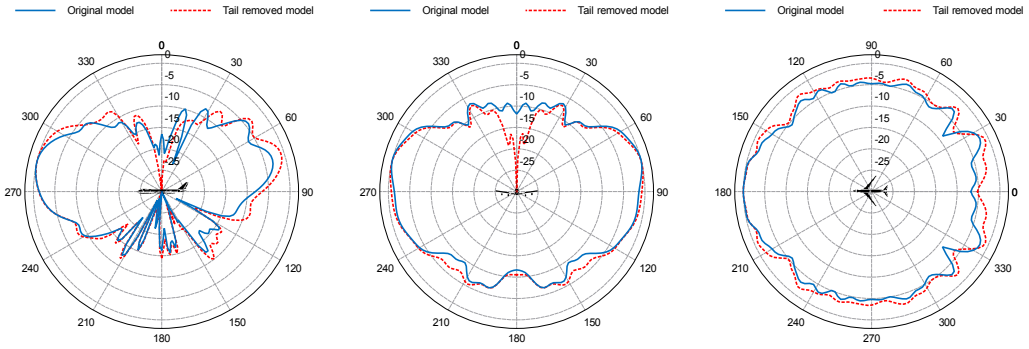

(a) (b) (c)

Figure 2.8: Radiation pattern of the model shown in Fig. 2.7a compared to the radiation pattern of the original model at 100 MHz in (a) pitch plane (b) roll plane (c) yaw plane.

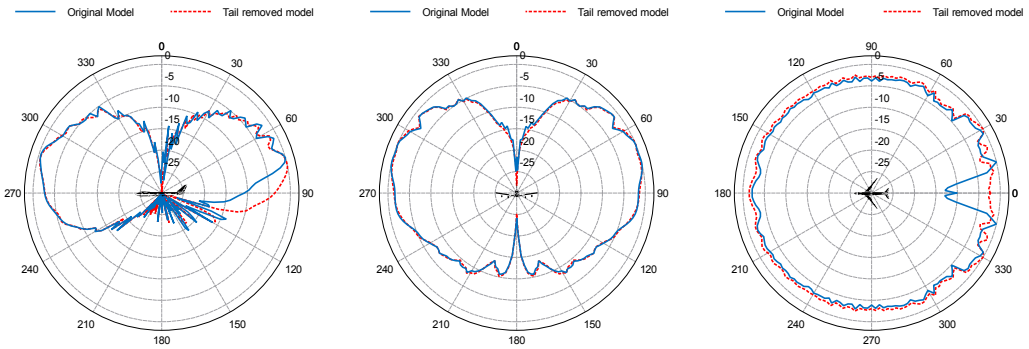

(a) (b) (c)

Figure 2.9: Radiation pattern of the model shown in Fig. 2.7a compared to the radiation pattern of the original model at 300 MHz in (a) pitch plane (b) roll plane (c) yaw plane.

2.1.1 Removing the Empennage

Fig. 2.7a shows the aircraft model with the empennage removed. The radiation pattern of the monopole on this model at 100, 300, 450 MHz is shown in Fig. 2.8, 2.9 and 2.10 respectively. The radiation pattern of the monopole on the original aircraft model is also shown for comparison.

As can be seen, the patterns in the pitch plane are similar in a large angular sector, but for the tail-removed model there is more coverage in the lower hemisphere under the tail since the tail blockage is removed. At 450 MHz, the fuselage becomes

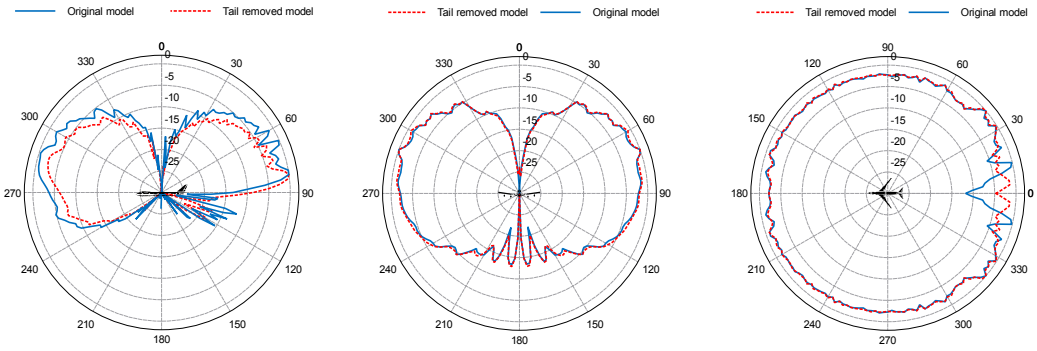

(a) (b) (c)

Figure 2.10: Radiation pattern of the model shown in Fig. 2.7a compared to the radiation pattern of the original model at 450 MHz in (a) pitch plane (b) roll plane (c) yaw plane.

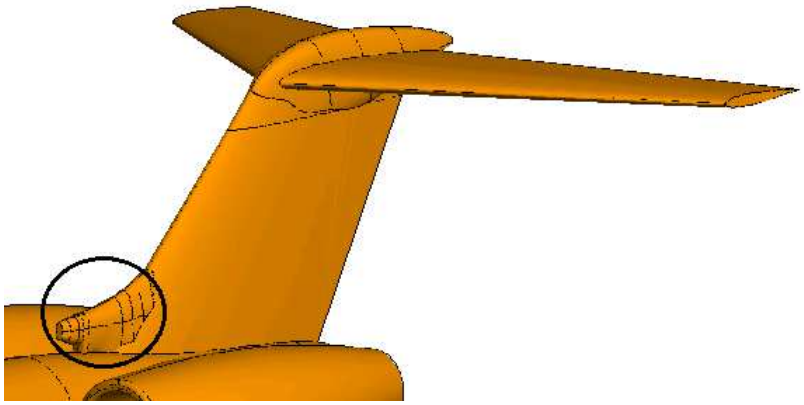

Figure 2.11: Empennage geometry.

electrically large enough to compensate for the blockage of the tail when it is removed. As a result, at this frequency the pitch patterns are very similar.

In the roll plane, the patterns are almost identical at the two higher frequencies. However, at 100 MHz, the patterns are different around the zenith direction. This means that in the roll plane, the scattering form the empennage is only influential around the zenith direction and at low frequencies where the empennage is electrically close to the antenna and is illuminated rather strongly. Further investigation shows that this scattering is mostly due to the bump in the base of the vertical stabilizer shown in Fig. 2.11.

In the yaw plane, the patterns are different at the tail side at two higher frequencies due to the empennage LOS blockage. The lack of this null at 100 MHz is due to the effective scattering from the engines that are electrically close to the antenna at this frequency.

2.1.2 Removing the Nose

Fig. 2.7b shows the aircraft original model with the nose removed. The radiation analysis of this structure is performed at 100, 300 and 450 MHz and the patterns in three principal planes are compared with the radiation patterns of the original model.

As can be seen in Fig. 2.12, 2.13 and 2.14, the patterns in roll and yaw planes at all the frequencies are very similar. The similarity increases as the frequency goes up. This is because as the frequency goes up the fuselage becomes electrically larger and the nose gets further away from the antenna. The pitch plane pattern, however, is affected by this change in the geometry since the nose blockage is gone and hence the radiation in the lower hemisphere has increased.

Note that although the monopole is located forward of the wings and hence closer to the nose than the empennage, removing the empennage tend to have a more drastic impact on the radiation of the antenna. This is a result of empennage LOS blockage

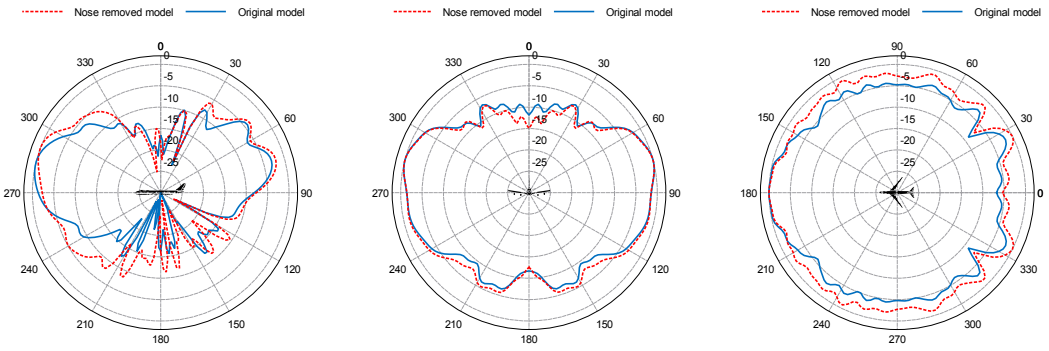

(a) (b) (c)

Figure 2.12: Radiation pattern of the model shown in Fig. 2.7b compared to the radiation pattern of the original model at 100 MHz in (a) pitch plane. (b) roll plane. (c) yaw plane.

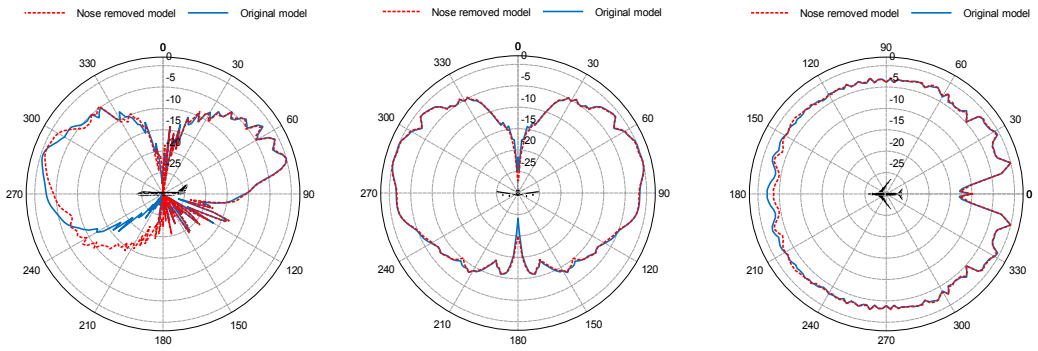

(a) (b) (c)

Figure 2.13: Radiation pattern of the model shown in Fig. 2.7b compared to the radiation pattern of the original model at 300 MHz in (a) pitch plane (b) roll plane (c) yaw plane.

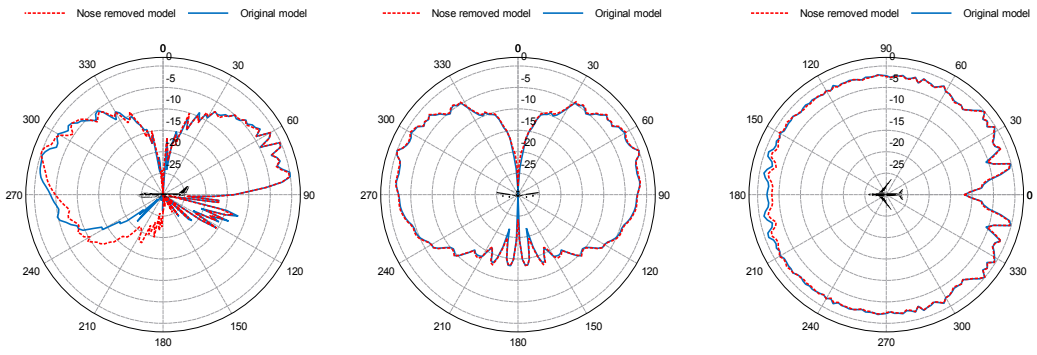

(a) (b) (c)

Figure 2.14: Radiation pattern of the model shown in Fig. 2.7b compared to the radiation pattern of the original model at 450 MHz in (a) pitch plane (b) roll plane (c) yaw plane.

as well as the direct illumination of the empennage from the antenna.

2.1.3 Removing the Wings

Fig. 2.7c shows the aircraft original model with the wings removed. The radiation analysis of this structure is performed at 100, 300 and 450 MHz and the patterns in three principal planes are compared with the radiation patterns of the original model.

As can be seen in Fig. 2.15, 2.16 and 2.17, the patterns in pitch and yaw planes at all the frequencies are very similar. The similarity increases as the frequency goes up and the electrical distance of the wings from the antenna increases.

In the roll plane, the patterns are very similar at the two higher frequencies. At 100 MHz, the patterns have the same general feature, but the pattern for the wings-removed model is smoother and does not have any ripples. This is due to the fact that the multipath interference due to the fields scattered from the wings, causing the ripples, is not present in the wings-removed model. At higher frequencies, the wings are less strongly illuminated and hence the scattering from the wings have lesser contribution to the radiation pattern.

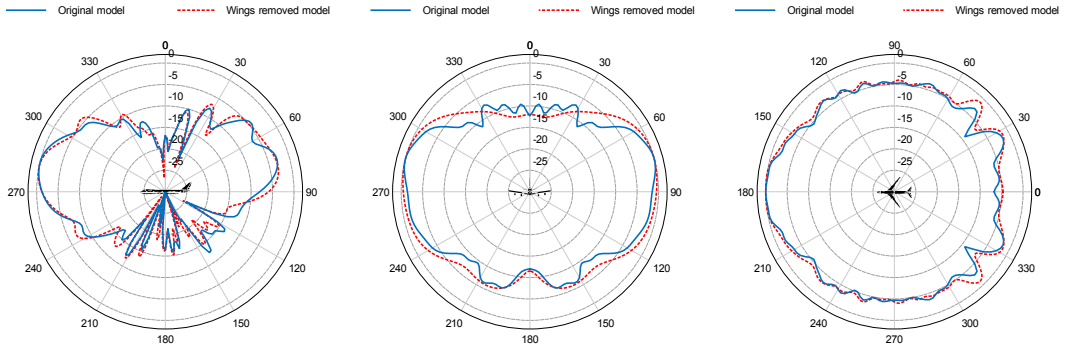

(a) (b) (c)

Figure 2.15: Radiation pattern of the model shown in Fig. 2.7c compared to the radiation pattern of the original model at 100 MHz in (a) pitch plane (b) roll plane (c) yaw plane.

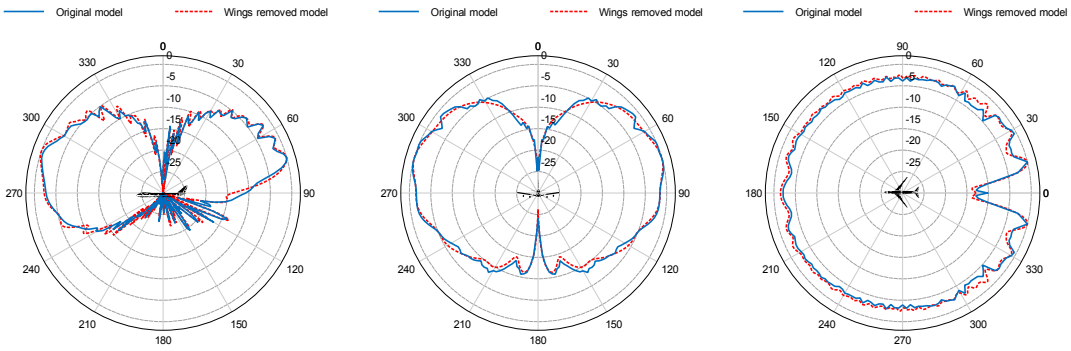

(a) (b) (c)

Figure 2.16: Radiation pattern of the model shown in Fig. 2.7c compared to the radiation pattern of the original model at 300 MHz in (a) pitch plane (b) roll plane (c) yaw plane.

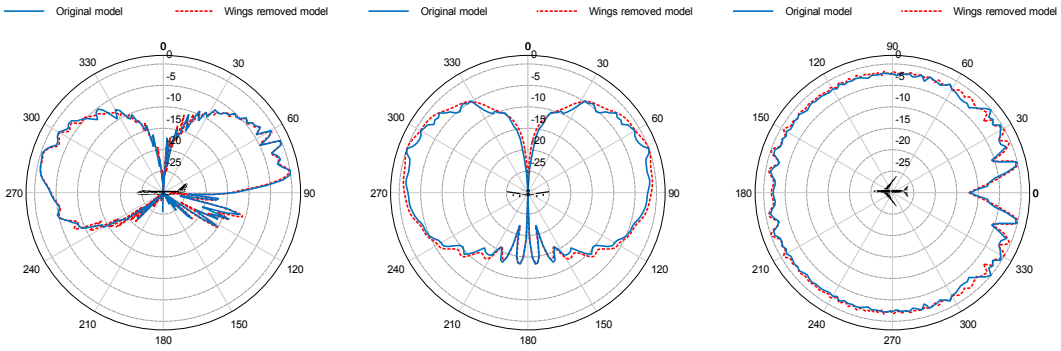

(a) (b) (c)

Figure 2.17: Radiation pattern of the model shown in Fig. 2.7c compared to the radiation pattern of the original model at 450 MHz in (a) pitch plane (b) roll plane (c) yaw plane.

2.1.4 Canonical Model

Fig. 2.7d shows a canonical model of the aircraft. The model contains only cylinders, spheroids and flat plates and is made using the drawing tools in Feko.

The patterns in principal planes are compared to the patterns of the original model at 100MHz and 300MHz in Fig. 2.18 and 2.19 respectively.

A canonical model can be made with the drawing tools provided in the EM modelling software tool. Moreover, a canonical model can be analyzed using the asymptotic high frequency technique, Uniform Theory of Diffraction (UTD).

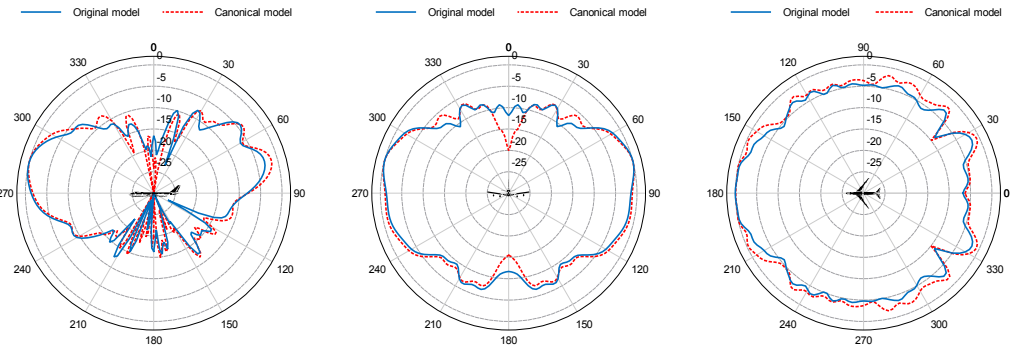

(a) (b) (c)

Figure 2.18: Radiation pattern of the model shown in Fig. 2.7d compared to the radiation pattern of the original model at 100 MHz in (a) pitch plane (b) roll plane (c) yaw plane.

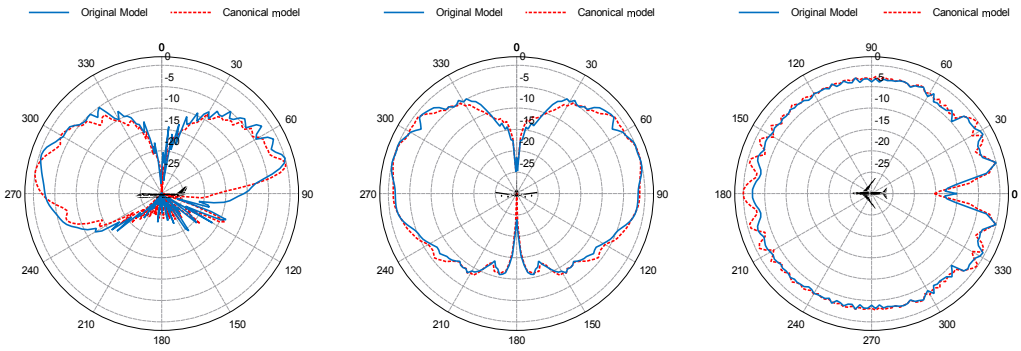

(a) (b) (c)

Figure 2.19: Radiation pattern of the model shown in Fig. 2.7d compared to the radiation pattern of the original model at 300 MHz in (a) pitch plane (b) roll plane (c) yaw plane.

These advantages are gained at almost no cost at the higher frequency where the pattern in the three planes is very similar to the original pattern. The pattern of the canonical model is just somewhat smoother and contain fewer ripples since fewer details are included in the simplified model.

At the lower frequency, however, there are deviations from the original pattern around the zenith. This is due to the fact that the modelling of the empennage using only plates is not accurate enough at low frequencies where the empennage is electrically close to the antenna and hence the scattering behavior of the simplified empennage does not exactly imitate the original scattering behaviour. More specifically, the base of the tail which was held responsible in section 2.1.1, is not modelled in the canonical model.

2.2 Input Impedance

The input impedance of an antenna mounted on an aircraft is modified by the structure in the vicinity of the antenna. When calculating the impedance of an aircraft antenna using wire grid modelling, the region close to the antenna needs to be modelled carefully. The details that need to be included is this region are greater than

the details required for radiation pattern calculation and hence a finer mesh in this region may be required for accurate impedance calculation. This means that a larger problem needs to be solved for calculating the impedance if the whole aircraft model is used. However, it appears that if the fuselage is fat enough, i.e. the diameter is greater than 0.05λ, then only half a wavelength of the airframe either side of the antenna needs to be included in the model and the calculated impedance will be a good approximation of the impedance of the antenna on the whole aircraft [25].

Fig. 2.20 shows the input impedance of the monopole on the aircraft compared to the input impedance of the antenna when only one wavelength of the structure either side of the antenna is included in the model.

For the chosen antenna position, one lambda extension of the geometry is more or less in the form of a cylinder at frequencies higher than 100 MHz. At lower frequencies, portions of the wings are also included. As can be seen, the agreement between the two curves is less than perfect at 30 MHz. At higher frequencies, however, the agreement is very good since the fuselage gets fatter.

Here, the simplified model is much smaller than the original model specially at higher frequencies. Using this simplified model the impedance of the antenna on the aircraft can be calculated in seconds.

Note that when using the MoM for calculating the impedance of a wire antenna, the calculated impedance depends on the wire radius and mesh size. Here, the wire radius is chosen to be 1.5 mm. The segment size on the monopole antenna and the edge size of the triangular patches modelling the airframe were chosen $\lambda/40$ and $\lambda/8$ respectively. These values were chosen so that mesh convergence is achieved. Further increase in the number of mesh elements will increase the computational burden and finally the MoM limit for mesh size to radius ratio will be reached.

Fig. 2.20 also shows the input impedance of the monopole antenna on an infinite ground plane. It is observed that as the frequency increases, the impedance of the

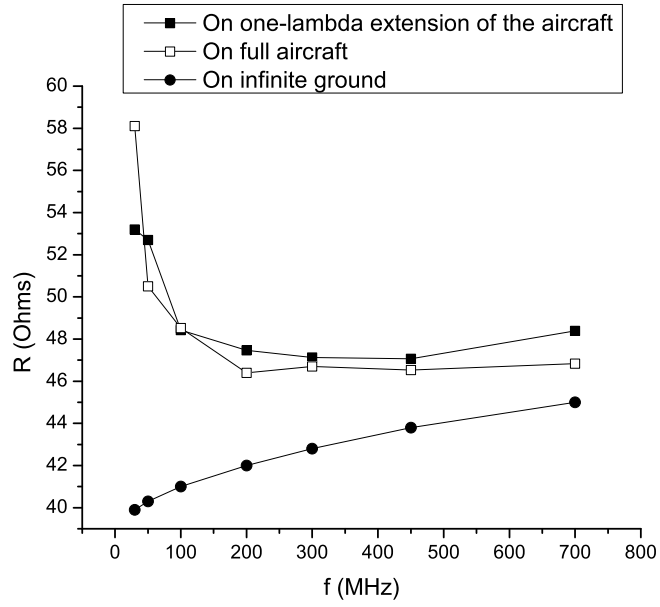

(a)

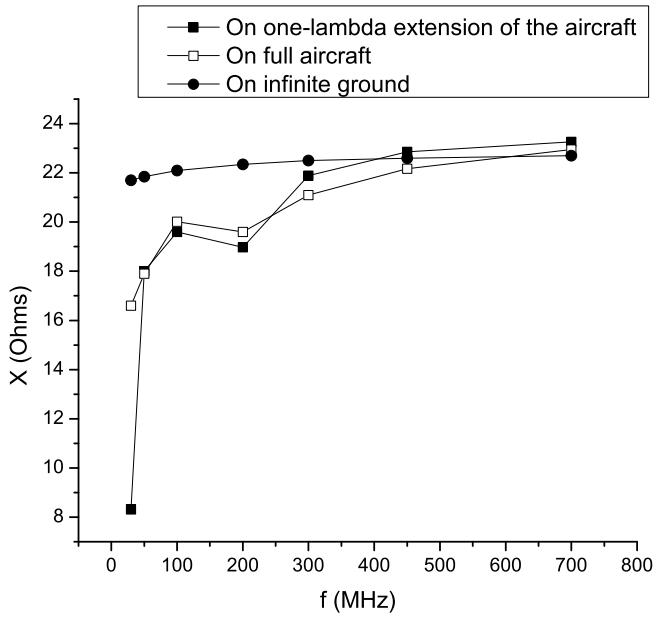

(b)

Figure 2.20: Input impedance of the antenna on the original model compared to the input impedance of the antenna on the simplified model and on infinite ground plane. (a) Real part. (b) Imaginary Part.

monopole on the aircraft approaches the impedance of a quarter-wave monopole on flat ground; at frequencies higher than about 450 MHz, the input impedance falls within 5% of the input impedance of a quarter-wave monopole antenna on an infinite ground plane.

On a peripheral note, as the frequency increases, the impedance of a quarter-wave monopole on an infinite ground plane (the impedance of a half-wave dipole divided by two) diverges from the value found in text books for a thin monopole, i.e. 36.5+j21.25 Ohms [24]. This is because as the frequency increases the 1.5mm radius of the wire gets electrically larger and the thin monopole assumption is not valid anymore.

2.3 Summary

It appears that scattering from parts of the aiframe mainly impact the radiation pattern at low frequencies where the electrical distance from the antenna is small. At high frequencies the impact of the airframe scattering is mostly in the form of small ripples in the pattern as the radiation pattern approaches the radiation pattern of the antenna on a flat ground plane.

However, contribution to the radiation pattern does not only depend on the electrical distance from the antenna. It was seen that due to direct normal illumination of the empennage from the antenna, the scattering from the empennage has a stronger contribution to the radiation pattern compared to the scattering from nose and wings even though the antenna was located closer to the nose and the wings than to the empennage.

The main features of the radiation pattern are preserved in the roll and yaw plane when the nose is removed with less than 4 dB change at all angles for frequencies higher than 100 MHz.

The wings can be removed if the radiation pattern at frequencies higher than

about 300 MHz is of interest and the calculated radiation pattern will be very similar to the original radiation pattern. At lower frequencies, the main features of the radiation pattern are still kept but in the roll plane the pattern is smoother and does not contain all the details.

However, not including the empennage in the CAD model can change the features of the radiation pattern at frequencies lower than 500 MHz: in the roll plane around zenith and in the pitch and yaw plane in the empennage side. Since the empennage is strongly illuminated by the antenna at low frequencies, even details of the empennage geometry need to be included and, as it was seen, a simplified canonical model of the empennage gives a radiation pattern which is not accurate around zenith at low frequencies.

For impedance calculations, including only one wavelength of the structure either side of the antenna is sufficient to calculate the antenna input impedance within reasonable accuracy for engineering applications.

Chapter 3

Numerical Techniques

The usefulness of a computer model greatly depends on its efficiency, accuracy and utility [26]. Modelling of the aircraft geometry and the numerical technique used for the analysis are the two factors that determine the above-mentioned characteristics. In Chapter 2, the impact of geometry modelling was studied. Here, the numerical techniques suitable for analysis of antennas on aircraft at VHF and UHF frequencies will be studied. A brief description of each technique is provided. Complications involved in using each technique are studied and numerical data on the computational resources required for each technique is provided. The computer used for this study is a HP Proliant DL360 G6 two quad-core machine with 72 GB RAM and CPU clock 2.93 GHz.

First, the MLFMM, a computationally efficient alternative to the traditional MoM, is studied. The MLFMM makes the full-wave analysis of antenna on electrically large structures, such as aircraft at VHF and UHF frequencies, possible. As will be seen, using the MLFMM, the radiation of a monopole antenna on the Bombardier aircraft can well be analyzed at frequencies up to 2 GHz in less than 3 hours.

At higher frequencies, asymptotic techniques such as Physical Optics (PO) and the Uniform Theory of Diffraction (UTD) can be employed. The asymptotic techniques

provide approximate solutions to Maxwell's equations using asymptotic expansions. As connoted by the word "asymptotic", the accuracy of these techniques improves as the frequency increases. These techniques are suitable for analysis of antennas on electrically huge structures.

The asymptotic techniques can be hybridised with full-wave methods to solve the problems which are intractable with the individual methods. Hybrid MoM/PO and MoM/UTD have been used for aircraft antenna analysis [27, 28].

Other techniques used for analysis of aircraft antennas include the Domain Decomposition Method (DDM) [29]. In DDM the domain is divided to several volume sub-domains. Each domain is then dealt with separately using the suitable technique and the sub-domains are characterized by the generalized scattering matrix. The added advantage of DDM is the ability to deal with collaborative studies and the reduced complexity in the context of parametric studies.

3.1 MLFMM

The Method of Moments (MoM) is a full-wave technique and can be applied to bodies of arbitrary shape. For radiation analysis of antennas on bulky and complex structures such as aircraft where the structure's surface to volume ratio is small, the Method of Moments (MoM) is more efficient compared to the finite volume methods, i.e. FDTD and FEM. In the MoM, the surface of the structure is modelled using patches or a wire-grid. One of the earliest attempts at aircraft modelling with the MoM can be found in [30].

In the MoM, the problem is formulated by an integral equation based on the Maxwell's equations. The respective integral equation is then converted to a system of linear algebraic equations. A dense matrix vector product needs to be performed to solve the system of linear equations and to find N unknowns, i.e. current on

mesh segments. This leads to $O(N^2)$ scaling of memory requirement and $O(N^3)$ scaling of CPU-time. The mesh segments should be electrically short since the current distribution is assumed linear over each segment. Thus, as the frequency increases and the wavelength gets smaller, a finer mesh is required to model the body and the number of unknowns increases. Soon, the computational limits are reached and MoM becomes impractical.

The Multilevel Fast Multipole Method (MLFMM) is a computationally efficient integral equation technique that allows full-wave analysis of electrically large structures that cannot be solved using the classic MoM. Using MLFMM, computational complexity is reduced from $O(N^2)$ to $O(NlogN)$ for memory requirement and from $O(N^3)$ to $O(Nlog^2N)$ scaling for CPU-time. This results in huge savings in computational resources at high frequencies.

The MLFMM cannot be considered a separate technique from the MoM since it is based on the same integral equation modelling of the physics. However, in the MLFMM unlike the MoM, only part of the impedance matrix is explicitly calculated. Rather, a process of aggregation, translation and disaggregation of different levels is employed for analytical decomposition of the impedance matrix, so that the computational complexity of the matrix vector product is reduced [31]. The MLFMM therefore needs to be used in iterative solutions of the matrix equations.

The radiation of a monopole antenna on the aircraft shown in Fig. 2.1 was analyzed at 100 MHz, using the MLFMM and MoM. The analyses were performed in Feko 6.1 using an 8-process parallel solver. The surface of the model is discretized to electrically small triangular patches. The Feko standard value for the triangle edge length, i.e. $\lambda/8$, is used. Table 3.1 compares the CPU-time and memory requirements for the two techniques. Note that "peak memory" refers to the sum of the peak memory of all processes. It is seen that employing MLFMM, the analysis can be performed at a significantly reduced computational cost. It should be noted that

	# of unknowns	Peak Memory	CPU-time
MLFMM	43290	2.54 GB	100 sec
MoM	43290	14.07 GB	42.6 min

Table 3.1: Comparison of computational resources required using the MLFMM with those required using the MoM, for analysis at 100 MHz.

the MLFMM results are in perfect agreement with the traditional MoM results.

3.1.1 Convergence

The MLFMM improves the computational efficiency of the MoM matrix vector product and therefore it needs to be used in iterative solutions. Convergence for the iterative solver, however, is not always easily obtained. The iterative solver might not converge or too many iteration counts might be required to achieve convergence.

As said earlier, the MLFMM is an integral equation technique. The choice of the integral equation formulating the problem impacts the convergence. The Electric Field Integral Equation (EFIE) formulation is the most general formulation since it can be applied to both closed and open metallic objects. The EFIE formulation, however, can lead to ill-conditioned matrix equations which in turn results in poor convergence.

Convergence of the iterative solution can be improved by employing the Combined Field Integral Equation (CFIE). The CFIE is a linear combination of the MFIE and EFIE with a factor, α. Choosing $\alpha = 1$ and $\alpha = 0$ reduces the CFIE to the EFIE and MFIE respectively. 0.2 is believed to be an optimal value for α [32]. The CFIE formulation leads to a better conditioned matrix and hence improves the solution convergence. Unlike EFIE, MFIE and hence CFIE formulations can only be applied to closed metallic bodies and also do not work well on surfaces with sharp edges or non-continuous curvature. Thus, the CFIE cannot be applied to all surfaces of our aircraft model since it contains many sharp corners.

Frequency	Formulation	# of unknowns	# of iterations	Peak memory	CPU-time
100 MHz	EFIE	43,290	46	2.54 GB	165 sec
	Hybrid CFIE-EFIE	43,290	11	2.54 GB	100 sec
450 MHz	EFIE	365,094	111	11.637 GB	11.8 min
	Hybrid CFIE-EFIE	365,094	80	12.297 GB	21.26 min
700 MHz	EFIE	854,367	102	28.05 GB	28.4 min
	Hybrid CFIE-EFIE	854,367	43	29.2 GB	31.4 min
1 GHz	EFIE	1,725,554	213	59.45 GB	2.9 hours
	Hybrid CFIE-EFIE	1,725,554	58	62.63 GB	51.4 min

Table 3.2: Solution convergence using hybrid CFIE-EFIE and EFIE.

This issue can be addressed by using the hybrid CFIE-EFIE formulation. Feko allows applying CFIE formulation to a subset of a problem. Thus, CFIE is applied to metallic faces comprising the cylindrical part of the fuselage and EFIE is applied to the remaining faces. Table 3.2 compares the MLFMM convergence for the EFIE and hybrid CFIE-EFIE formulations at different frequencies. Note that both formulations converged to the same solution.

It can be observed that at all frequencies, the hybrid CFIE-EFIE requires a fewer number of iterations. At 1 GHz, this leads to great reduction in the overall CPU-time needed for the analysis. This shows that employing the CFIE can make a big difference at high frequencies where slow convergence of the EFIE can prolong the analysis by hours. Note that although the hybrid CFIE-EFIE improves the MLFMM convergence, the calculation of matrix elements and preconditioning of the matrix takes longer in Feko when the hybrid CFIE-EFIE is used. As a result, at lower frequencies where the overall analysis does not take long, the EFIE solution can be more efficient.

The choice of the pre-conditioner also impacts the MLFMM convergence. The Feko 6.1 default pre-conditioner for parallel MLFMM is called Super-LU, whereas the previous versions of Feko used the Sparse Approximate Inverse (SPAI) pre-conditioner as the default pre-conditioner. The Super-LU pre-conditioner leads to better convergence and can be faster compared to the SPAI pre-conditioner, but it is less sparse

Pre-conditioner	# of unknowns	# of iterations	Peak memory	CPU-time
Super-LU	1,725,554	58	62.63 GB	51.4 min
SPAI	1,725,554	161	21.94 GB	1.31 hours

Table 3.3: Solution convergence at 1 GHz, using the SPAI and Super-LU pre-conditioner.

and hence uses more memory. At frequencies where the memory limit is reached with the Super-LU pre-conditioner, the SPAI pre-conditioner can be used to increase the MLFMM problem size limit. This, of course, is achieved at the cost of slower convergence and longer simulation run, as can be seen in Table 3.3.

Other ways to improve convergence for the parallel MLFMM includes slightly changing the mesh size or the MLFMM minimum box size, but these trial-and-error approaches are impractical at high frequencies where the problem size is electrically large.

3.1.2 Meshing

In the MoM and hence MLFMM, the structure is modelled using wire segments or patches over which the current can be assumed piecewise linear. This implies that the mesh segments need to be electrically small. For general structures, a linear dimension of the order of 0.1 wavelength is recommended for each segment [25].

This means that at very low frequencies where the aircraft is electrically small, the airframe can be modelled with a stick model, i.e. the fuselage and wings can be simply modelled using wire segments [33]. However, as the frequency increases, a finer mesh containing more details of the geometry is required to model the aircraft and number of unknowns increases rapidly with the electrical size of the object.

In Feko, the airframe is modelled using triangular patches [34]. Fig. 3.1 shows the aircraft simulation mesh at 100 MHz. The number of unknowns equals the number of internal triangle edges (edges that belong to two triangles) which is roughly 1.5

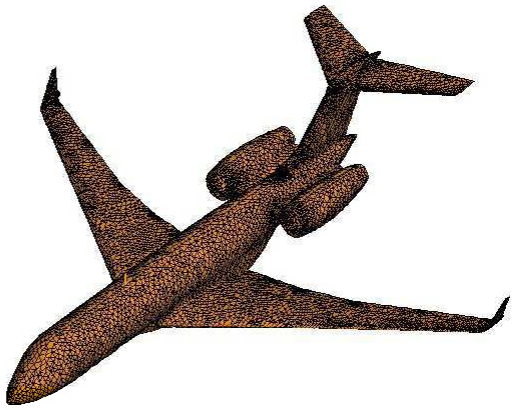

Figure 3.1: Aircraft simulation mesh at 100 MHz.

times the number of triangles.

In the case of a complex structure such as an aircraft, it is not easy to calculate the total number of unknowns that would result from the meshing of the CAD model. Inspired by the formulas presented in Chapter 7 of [13], the following empirical formula is derived for the Bombardier aircraft. $\#\ of\ unknowns = 2.7 \times 10^{-14} \times c^2/d^2$. This formula can be used to estimate the number of unknowns that would result from meshing the CAD in Feko. d is the segment length and c is the speed of light.

The Feko default value for the triangle edge length is $\lambda/8$. However, the $\lambda/5$ triangle edge length is seen to be sufficiently accurate even for input impedance calculations. Fig. 3.2 shows the normalized gain pattern at 1 GHz for meshes with $\lambda/5$ and $\lambda/8$ triangle edge length. As can be seen, for all practical purposes the two results are identical. The input impedance of the $\lambda/5$ edge length model differs from input impedance of the $\lambda/8$ edge length model only by 3%. Computational resources required for analysis at 1 GHz for meshes with $\lambda/5$ triangle edge length and $\lambda/8$ triangle edge length are compared in Table 3.4.

The radiation pattern at 2 GHz, discussed in Chapter 2 (Fig 2.6), was obtained using $\lambda/5$ triangle edge length. The 2,683,949 unknowns were solved in 2.87 hours

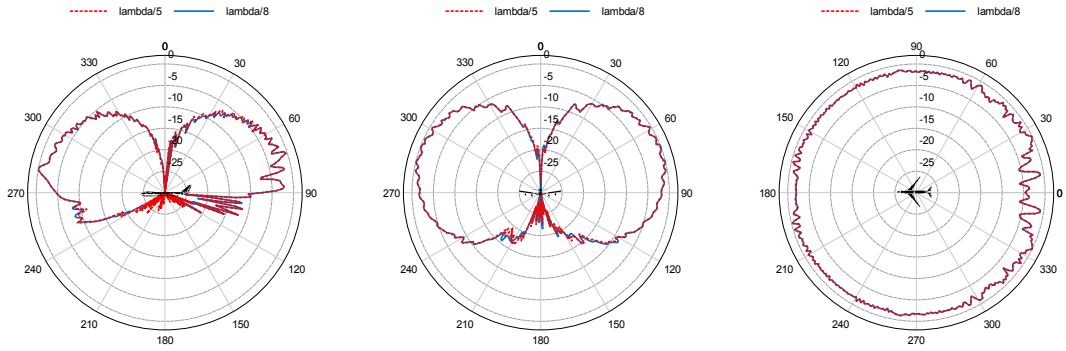

(a) (b) (c)

Figure 3.2: Radiation pattern obtained using mesh with $\lambda/5$ triangle edge length compared to the radiation pattern obtained using mesh with $\lambda/8$ triangle edge length, at 1 GHz (a) pitch plane. (b) roll plane. (c) yaw plane.

Triangle edge length	# of unknowns	Peak Memory	CPU-time
$\lambda/8$	1,725,554	62.63 GB	51.4 min
$\lambda/5$	687,221	16.4 GB	41.68

Table 3.4: Computational resources required for analysis at 1 GHz for meshes with $\lambda/8$ and $\lambda/5$ triangle edge lengths.

with a peak memory of 66.8 GB. Using $\lambda/8$ triangle edge size at 2 GHz, we ran out of memory.

For analysis at higher frequencies a coarser mesh can be used, but the accuracy of the results might be impacted. A nonuniform mesh can be used to reduce the problem size without hurting the accuracy. A finer mesh can be used in areas close to the antenna and regions that are strongly illuminated and a coarser mesh can be used in other regions.

3.2 Physical Optics

Physical Optics (PO) is an asymptotic high frequency technique. Like the MoM, PO is a current-based technique and can be applied to bodies of arbitrary shape. In the PO formulation, however, the currents on the metallic surfaces are simply calculated from the GO fields. Diffraction is only approximately treated in PO.

Feko hybridises PO with MoM where MoM current elements are used to excite computationally inexpensive PO elements. PO was applied to the airframe while the monopole was treated with the MoM. The analysis was performed at 100 MHz, 450 MHz and 1 GHz. The gain patterns are shown in Fig. 3.3 to 3.5. The gain patterns obtained using MLFMM are also shown for comparison.

As can be seen in Fig. 3.3, at 100 MHz, the PO pattern differs from the MLFMM pattern specially in the zenith direction. There are also differences in the lower hemisphere especially in the tail side. This is due to the fact that diffraction is only approximately considered in PO. Thus, PO radiation pattern solutions lack accuracy at low frequencies. However, as the frequency increases, the accuracy improves. At 450 MHz and 1 GHz, the PO pattern is in a good agreement with the MLFMM pattern. There are still fewer ripples in the PO pattern due to lack of higher order interactions and there are also differences in the shadow region for the same reason. However, by using PO at these frequencies, a good knowledge of the radiation pattern is obtained at a significantly reduced computational cost. Table 3.5 shows the CPU-time and memory requirements for PO. Comparing Table 3.5 with Table 3.2, it is seen that the memory required for PO is significantly less than the memory required for MLFMM.

As a result, PO is a suitable technique for analysis at high frequencies where the aircraft becomes electrically very large and analysis with MLFMM is not possible.

Note that one needs to be careful when using PO for impedance calculations. As the frequency increases, the accuracy of the real part of the calculated input impedance increases. However, the calculated value for the imaginary part cannot be trusted. For a more accurate impedance calculation, the hybrid MoM/PO can be applied to the airframe. The triangle patches in the region close to the antenna can be treated using the MoM and PO can be applied to the rest.

Fig. 3.6 shows the current density on the airframe at 450 MHz, calculated using

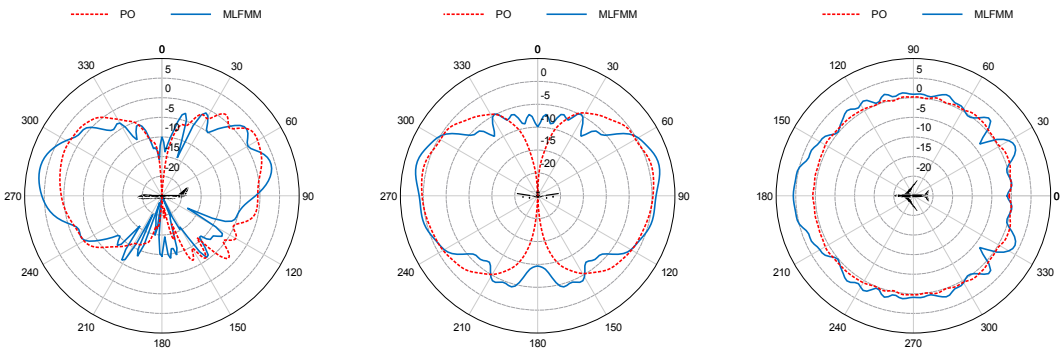

(a) (b) (c)

Figure 3.3: Radiation pattern obtained using PO compared to the radiation pattern obtained using MLFMM, at 100 MHz (a) pitch plane. (b) roll plane. (c) yaw plane.

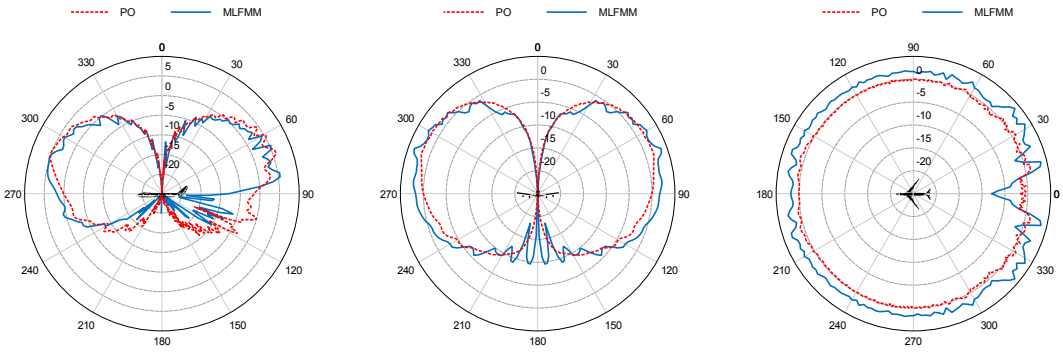

(a) (b) (c)

Figure 3.4: Radiation pattern obtained using PO compared to the radiation pattern obtained using MLFMM, at 450 MHz (a) pitch plane. (b) roll plane. (c) yaw plane.

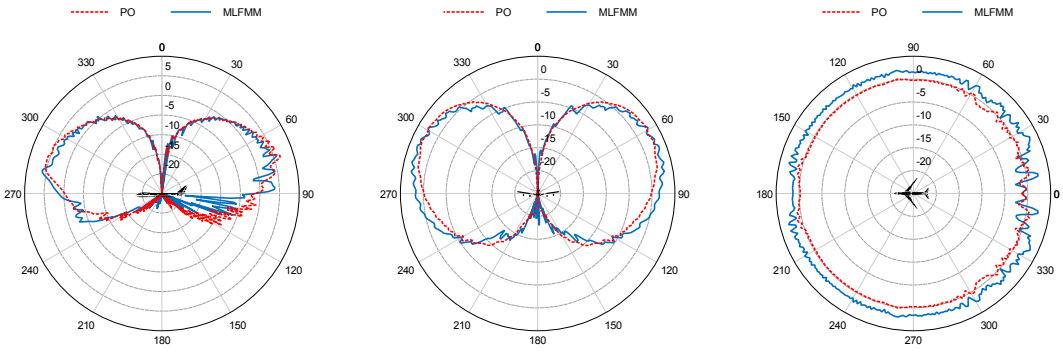

(a) (b) (c)

Figure 3.5: Radiation pattern obtained using PO compared to the radiation pattern obtained using MLFMM, at 1 GHz (a) pitch plane. (b) roll plane. (c) yaw plane.

Frequency	# of unknowns		Peak Memory	CPU-time
	# of MoM basis funct.	# of PO basis funct.		
100 MHz	12	43,278	130.8 MB	76.2 sec
450 MHz	12	365,082	1.05 GB	15 min
1 GHz	11	1,725,543	4.84 GB	44.77 min

Table 3.5: Computational resources required using PO.

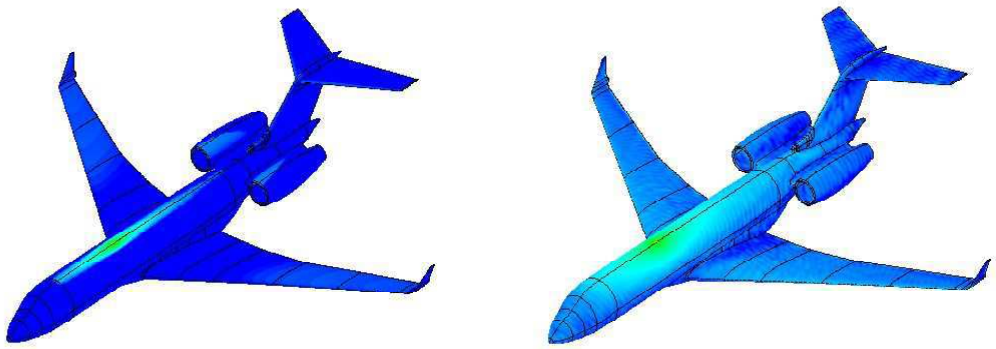

(a) (b)

Figure 3.6: Current density on the airframe at 450 MHz (a) calculated using PO (b) calculated using the MLFMM.

PO and MLFMM. There are abrupt discontinuities in the PO current and the current densities look distinctly different. Nevertheless, when the radiation integrals are applied to these two distinct-looking surface currents to calculate the radiated field, the difference diminishes and, as stated earlier, the radiation patterns calculated using the MLFMM and PO are similar at 450 MHz.

3.3 Uniform Theory of Diffraction

The Uniform Theory of Diffraction (UTD) is based on an asymptotic high frequency solution of Maxwell's equations. UTD can be used to treat electrically large structures consisting only of canonical shapes. In UTD, the electromagnetic waves are considered as rays subjected to reflection and also diffraction to include the effect of tips, edges and creeping waves.

For electrically large objects, reflection and diffraction are essentially local phenomena and therefore increasing the problem size does not increase the computational complexity. The memory and CPU-time requirement are therefore frequency independent for UTD and this technique is very well suited for analysis of aircraft antennas at high frequencies where the full wave analysis cannot be afforded.

UTD is based on high frequency assumptions: No linear dimension, d, can be less than lambda ($2\pi d/\lambda \gg 1$) and the source and various scattering centers need to be separated on the order of a wavelength or more [35]. For a monopole antenna on the fuselage of the Bombardier aircraft this translates to frequencies greater than about 100 MHz. Note that simplified canonical models of the airframe need to be used, according to the antenna location and the plane in which the radiation pattern is of interest.

Fig. 3.7, shows the first order UTD interactions that contribute to the radiation for an antenna on top of the fuselage of an aircraft. Other than the first order interactions, there also exists higher order interactions. The intensity of a ray is reduced as it goes through multiple interactions and hence the higher order interactions have a lesser contribution to the radiation. Table 7.2 in [13] shows the ratio of different interactions. Including the higher order interactions in the calculation increases the complexity of the technique. Moreover, errors due to not including the higher order terms merely result in amplitude jumps in the radiation pattern at some angles. This indicates that the higher order terms are only important at some angular sectors detected by the amplitude jumps.

UTD can be applied solely for analysis of wire or slot antennas on the fuselage. However, in case of more complicated antennas (such as microstrip), other computational methods (like FEM) or theoretical models need to be hybridised with UTD to determine the antenna radiation. Furthermore, for some antenna positions such as the tail where the requirements of UTD are not met, the MoM can be used to model

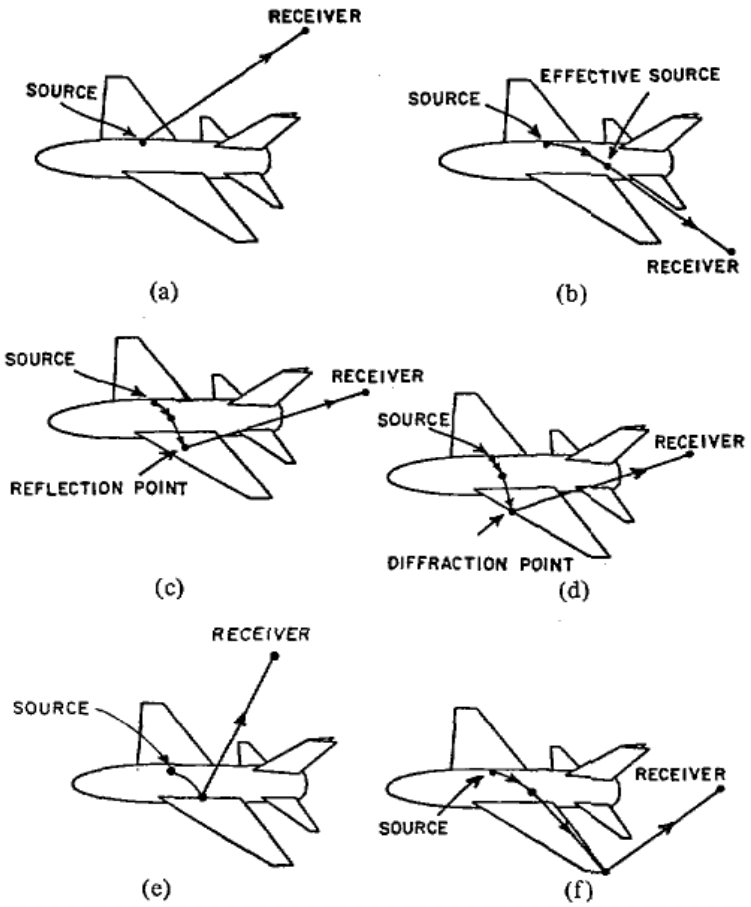

Figure 3.7: Various first-order UTD interactions (a) Direct source field. (b) Effective source field. (c) Reflected field. (d) Edge diffracted field. (e) Curved junction edge diffracted field. (f) Corner diffracted field. [2]

the region around the antenna and UTD can be applied to the rest of the airframe.

3.3.1 Radiation Pattern

The roll plane far-field radiation pattern of a quarter-wave monopole antenna on a cylinder was calculated using UTD. The direct ray and the two first-order tangentially-shed rays were considered in the pattern calculation, as shown in Fig. 3.8. The UTD solution described in [36] was used for the ray fields.

The cylinder, modelling the airframe, has radius of 1.38 m and analysis is performed at 300 MHz. Fig. 3.9 shows the gain pattern compared to the roll plane

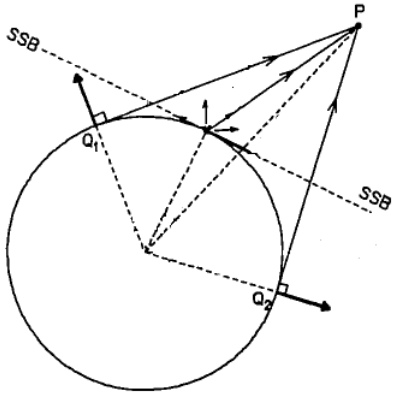

Figure 3.8: Interactions included in the calculation of the roll plane pattern, taken from [3] with modifications.

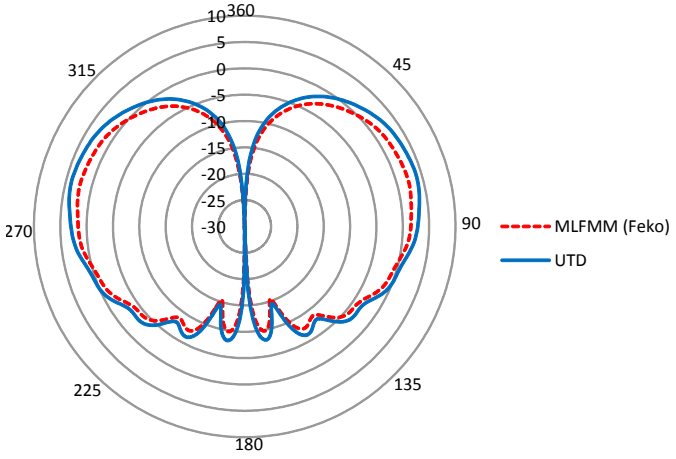

Figure 3.9: Roll plane radiation pattern for a quarter-wave monopole on a cylinder modelling the airframe at 300 MHz.

pattern of a quarter-wave monopole on a 26 m long cylinder calculated in Feko, using the MLFMM. As can be seen the two results have the same features and are less than 3 dB different at all angles.

The airframe can be validly modelled by a cylinder to calculate the roll plane radiation pattern of a monopole located forward of the wings at 300 MHz. However, other portions of the aircraft might need to be included in the model for other antenna positions or at other frequencies or if the radiation pattern in some other plane is of interest. The study conducted in Chapter 2 helps with deciding which details of the

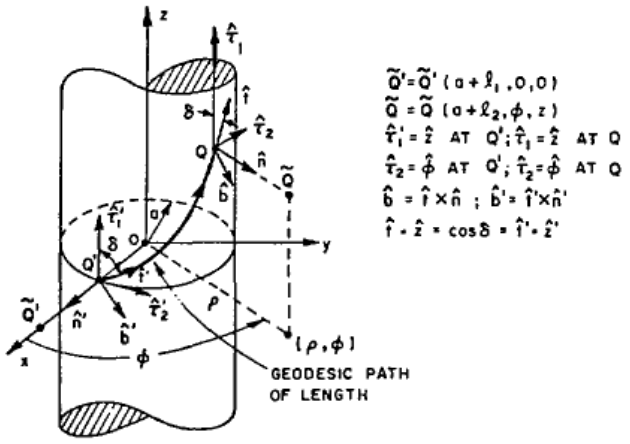

Figure 3.10: The cylinder geometry for mutual coupling calculation [4].

geometry need to be included in the model.

3.3.2 Coupling

There are several antenna systems on an aircraft. The power radiated by one antenna system can be received by another system. The coupling between two antennas is defined as the ratio of the received power (in a matched load) and the radiated power [25]. Note that the impedance mismatches and losses due to cables and connectors are not considered in calculating the coupling between two antennas. It is desired that coupling between antennas on aircraft be minimized for effective simultaneous operation of the antenna systems.

The mutual coupling between two antennas on aircraft can be calculated using UTD. In [4], a UTD solution for the EM field induced on the surface of a metallic cylinder due to a short monopole on the cylinder is described. The solution is expressed in terms of Fock integrals which are tabulated. Knowing the field on the cylinder, the reaction theorem [37] is then used to calculate the mutual impedance between two short monopoles located at Q and Q' shown in Fig. 3.10.

Fig. 3.11 shows the mutual coupling between short (0.1λ long) monopoles on the cylinder versus ϕ, for $\delta = 90$ and 45 deg. δ is the angle subtended between the

cylinder axis (z axis) and the geodesic path. The radius of the cylinder, a, is 1.6λ ($ka = 10$) which corresponds to the fuselage radius at about 350 MHz.

The mutual coupling between two short monopoles on a cylinder ($a = 1.6\lambda$) was also calculated in Feko, using the MLFMM, and is shown for comparison. The cylinder length was chosen 20λ since further increasing the cylinder length would not impact the results. As can be seen, the two results are in close agreement. Thus, UTD can be used to validly calculate the mutual coupling between antennas on the fuselage.

Alternatively, the following formula can be used to calculate the mutual coupling when the two antennas are in each other's far field regions, i.e., $t \gg 1.6\lambda (\phi \gg 57.2^0)$:

$$Coupling = \frac{P_r}{P_t} = G_t G_r (\frac{\lambda}{4\pi t} \mid V(\xi) \mid)^2$$

The above formula is derived from the UTD solution presented in [4] when only the highest order term is retained. This formula can be thought of as an extension of the Friis transmission formula [24] where $V(\xi)$ is a modification factor to include the effect of the curved geodesic path (of length t) that the wave travels from the transmitting to the receiving antenna. $\xi = (\frac{ka \times sin\delta}{2})^{\frac{1}{3}}\phi$ for a cylinder. $V(\xi)$ is the hard surface Fock integral tabulated in [38]. G_t and G_r are the gain of the equivalent short dipoles in the horizon, i.e., 1.5 (1.76 dBi).

The values of coupling calculated using the modified Friis formula are compared with Feko and UTD results in Table 3.6, for several values of ϕ.

As can be seen, the three results are in agreement with the maximum difference being less than 3 dB. The proposed formula provides a quick and easy means of calculating the coupling between antennas on the fuselage. This is very favorable due to the large number of antenna systems on aircraft, especially at the early stages of the design where the positions of antennas are constantly changing.

As may have been noticed, the airframe is modelled by a cylinder and other sections of the airframe are not included for the coupling analysis. This does not

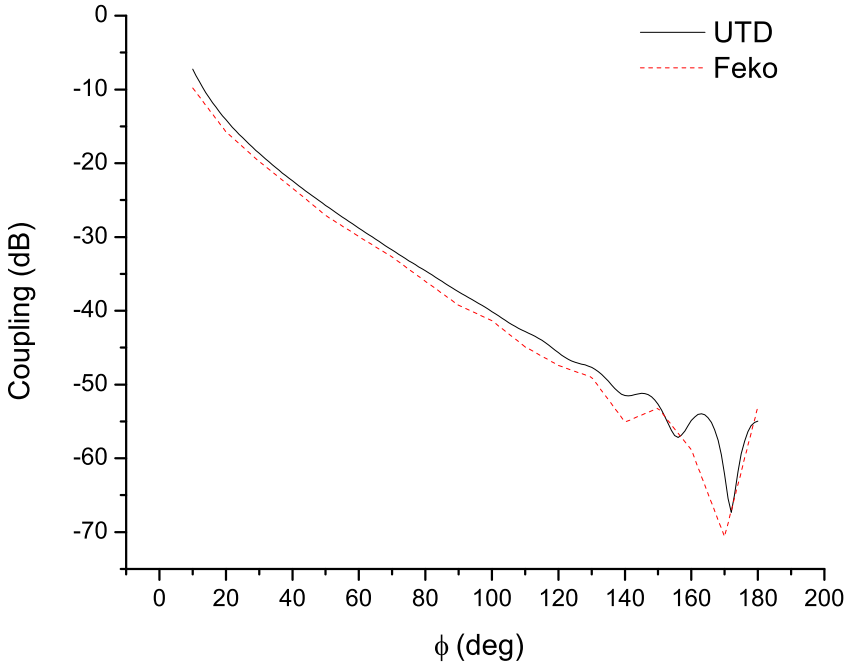

(a)

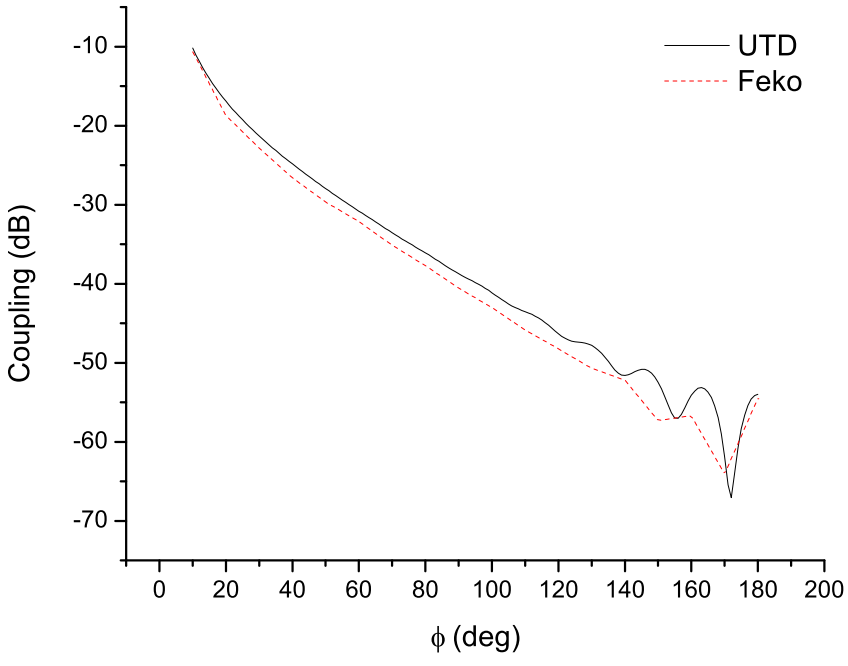

(b)

Figure 3.11: Coupling between two monopole antennas on a cylinder ($ka = 10$) (a) $\delta = 90°$ (b) $\delta = 45°$.

ϕ(deg)	Modified Friis Formula (dB)	UTD (dB)	Feko (dB)
70	-32.68	-31.77	-32.72
80	-35.89	-34.59	-36.01
90	-37.54	-37.44	-39.261
120	-43.95	-45.69	-47.39
150	-50.74	-52.68	-53.17
180	-54.97	-54.96	-53.05

(a)

ϕ(deg)	Modified Friis Formula (dB)	UTD (dB)	Feko (dB)
70	-33.27	-33.545	-35.12
80	-37.04	-36.1	-37.71
90	-40.89	-38.74	-40.55
120	-46.84	-46.34	-48.22
150	-56.00	-52.45	-57.31
180	-56.57	-53.98	-54.52

(b)

Table 3.6: Comparison of coupling values calculated using the modified Friis formula with UTD and Feko results. (a) $\delta = 90°$ (b) $\delta = 45°$.

pose a problem: When the two antennas are on the same side of the fuselage (both on the top or both on the bottom), other sections of the airframe like wings do not contribute significantly to the coupling between the antennas. When the antennas are on the opposite sides, the calculated result errs on the side of caution since including the wings would provide additional shading.

Chapter 4

Composite-Metal Junctions

Metal in different portions of some recent aircraft has been replaced by Carbon Fiber Composite (CFC) materials. In partially composite aircraft, metal (aluminum) and composite are placed in proximity to each other. The electrical conductivity of composite ($10^4 S/m$) is different from that of aluminum ($10^7 S/m$). The proximity of composite to metal may impact the antenna radiation since the change in the conductivity distorts the current density. This issue is investigated in this chapter.

In order examine the effect of vicinity to metal-CFC junctions on the antenna radiation, the simple case of a monopole antenna on a flat ground plane is considered. Due to the simplicity of the structure, the matter can be fundamentally studied.

A quarter-wave monopole, operating at 30 MHz, is placed on a half-CFC, half-aluminum 3-mm-thick square ground plane using surface-impedance model, as shown in Fig. 4.1. The ground plane is 3m long on each side.

At 30 MHz, the antenna is located in $\lambda/100$ distance from the boundary. Fig. 4.2 shows the current distribution on the plane and compares it to the current distribution on a full-aluminum plane.

As can be seen, in the vicinity of the junction the current density is distorted. The impact of this distortion is merely a slight change in the input reactance, leading

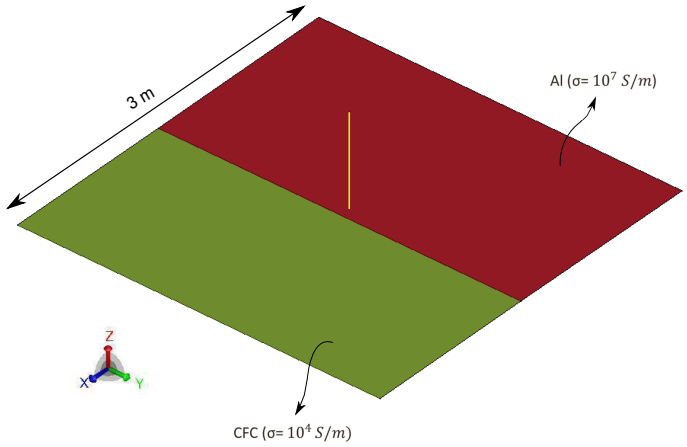

Figure 4.1: A quarter-wave monopole on a half-CFC, half-aluminum square ground plane.

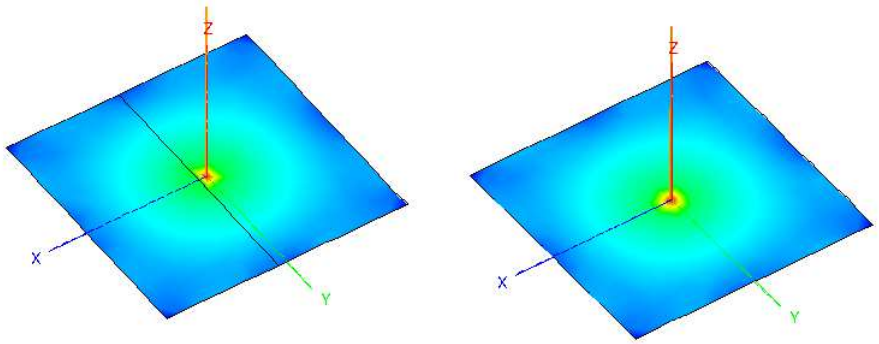

(a) (b)

Figure 4.2: Current density at 30 MHz (a) on the half-CFC, half-aluminum ground plane (b) on the full-aluminum ground plane.

to a 11% change in the antenna input impedance.

As can be seen in Fig. 4.3, there is no distortion in the radiation pattern. At higher frequencies, the electrical distance from the boundary is larger and hence the current density is less distorted. The impact on the antenna impedance is minimal.

It appears that vicinity to $10^4 S/m$ conductivity does not impact the antenna radiation and a much lower conductivity (in the order of $10\,S/m$) is required to see significant changes in the antenna radiation pattern and input impedance.

Note that due to the 1000 times lower conductivity of composite, the skin depth for composite is about 30 ($\sqrt{1000}$) times greater than that of the aluminum. This issue

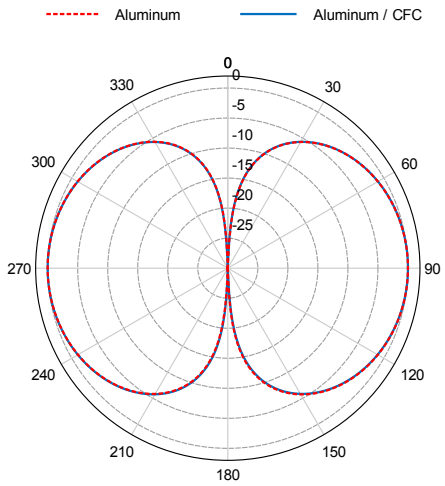

Figure 4.3: Normalized gain pattern at 30 MHz in the xz plane.

may also impact the radiation pattern when the ground plane is thin. To investigate this issue, the thickness of the ground plane was reduced. Only when the thickness is reduced to 5 μm, the two radiation patterns become slightly different at 30 MHz. At VHF and UHF frequencies, the skin depth of both composite and aluminum is too small to have any effect on the radiation pattern for ground planes with practical thicknesses. The skin depth of composite at 30 MHz, 100 MHz and 1 GHz is 918.8 μm, 503.2 μm and 159.1 μm respectively whereas the skin depth of aluminum at 30 MHz, 100 MHz and 1 GHz is 29 μm, 15.9 μm and 5.03 μm respectively.

Chapter 5

Cracks and Seams

An issue concerning the use of carbon-fiber composite materials in aircraft structures is the occurrence of cracks in the airframe and their impact on the aircraft antenna performance. Cracks may occur during fabrication and service life of these materials for various reasons. These cracks grow and develop and may join each other. The flow of the current is impeded where the fibers are broken and hence the antenna performance can be impacted by the cracks.

In addition to cracks, there are other discontinuities in the airframe due to doors, seams and joints. Fig. 5.1 shows some typical discontinuities in the airframe. There are also other less obvious discontinuities such as those being hidden by non-conductive fairings. These structural discontinuities, which exist in both metal and composite airframe, also impede the current flow on the surface of airframe and affect the antenna performance.

The discontinuities can be treated as parasitic slots if earthed at each end and as parasitic notches if they occur at the edges. Parasitic notches can have more significant effects on the antenna performance when resonant since the current density at the edges is high. In [5], Burberry shows the large impact of a resonant parasitic notch on a fin-cap antenna. However, the notches do not pose any issue to the

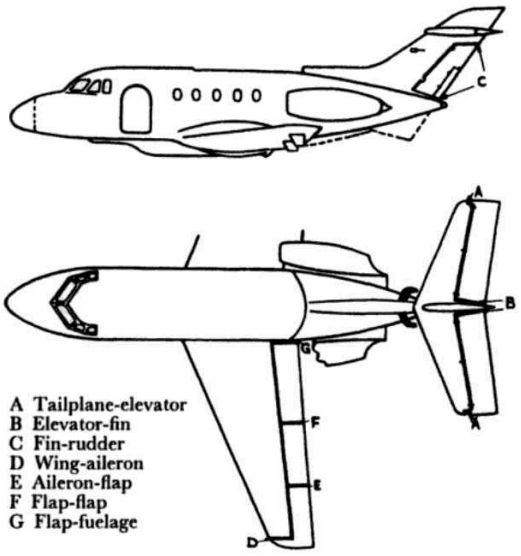

Figure 5.1: Typical discontinuities in the airframe [5].

fuselage-mounted antennas as they are not electrically close to these antennas at VHF and UHF frequencies.

In order to investigate the effect of the cracks and discontinuities on the radiation of a fuselage mounted antenna, the simple case of a monopole antenna on a flat ground plane is studied as the simplicity of this structure allows for a clear observation of the impact of cracks on the antenna radiation. The structure of a quarter-wave monopole on a square ground plane is shown in Fig. 5.2a. The ground plane is 4λ long on each side. Cracks of different sizes and at different distances from the antenna are introduced in the ground plane as shown in Fig. 5.2b. The round shape of the crack is suitable for this analysis since the current distribution on the ground plane is known to be radial, so a crack in the radial direction would not disturb the current flow and hence the antenna radiation. The impact of introducing cracks on the monopole radiation pattern and input impedance is studied.

Fig. 5.3 shows the normalize gain pattern for cracks with different arc lengths when $d = 0.5\lambda$ and $w = 0.05\lambda$. The radiation pattern of a monopole on a standard ground plane is also shown for comparison. As can be seen, the pattern in the upper hemisphere only slightly changes when the crack is symmetrical around the antenna

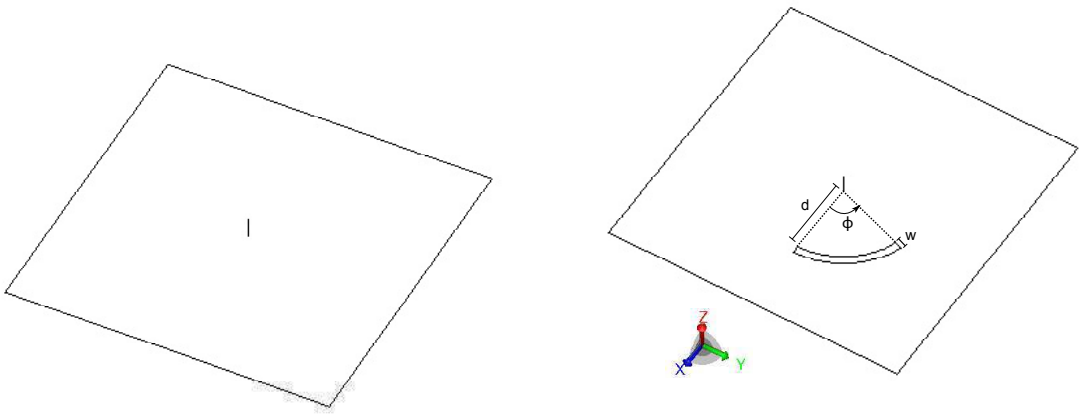

(a) (b)

Figure 5.2: Quarter-wave monopole antenna on a square ground plane (a) without cracks (b) with cracks.

(Fig. 5.3a).

In Fig. 5.3b and Fig. 5.3c, the pattern is distorted in the upper hemisphere especially around the zenith direction since radiated waves from different portions of the crack do not cancel out due to asymmetry. The asymmetrical cracks also damage the omnidirectionality of the antenna by causing asymmetry in the pattern.

Fig. 5.4 shows the normalized gain pattern for different values of crack width when $d = 0.5\lambda$ and the crack completely surrounds the antenna ($\phi = 360°$). In the three cases, the antenna radiation in the upper hemisphere is only slightly changed. Increasing the width results in slightly increased radiation in some angular sectors in the upper hemisphere.

Fig. 5.5 shows the normalized gain pattern for different values of d when $w = 0.05\lambda$ and the crack is symmetrical around the antenna ($\phi = 360°$).

When the crack is placed close to the antenna (Fig 5.5a and Fig. 5.5b), the radiation pattern in the upper hemisphere is only slightly distorted. This is justifiable since, disregarding the finite size of the ground plane, Babinet's/Booker's principle [39] can be applied to conclude that the field radiated by the annular crack is the

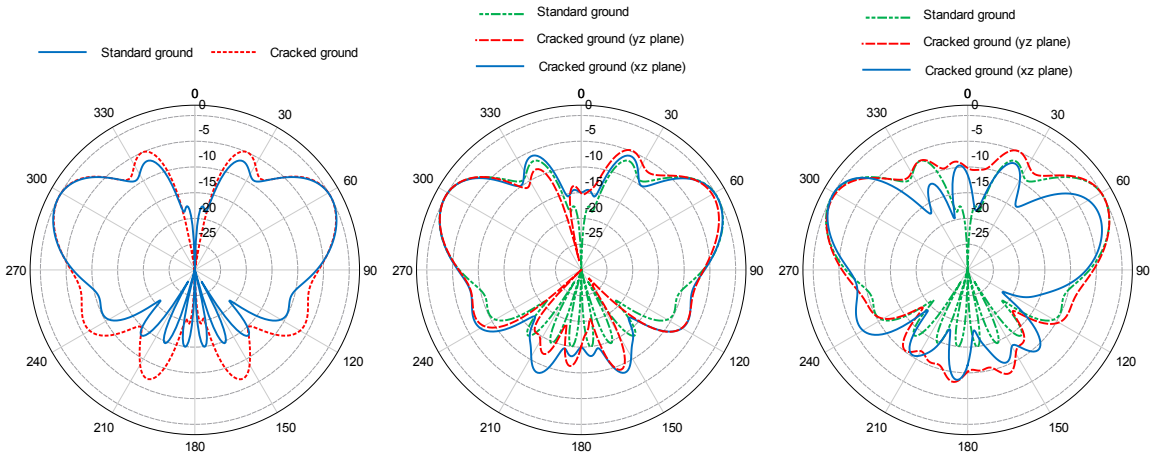

(a) (b) (c)

Figure 5.3: Radiation pattern when $d = 0.5\lambda$, $w = 0.05\lambda$ and (a) $\phi = 360°$ (b) $\phi = 180°$ (c) $\phi = 45°$.

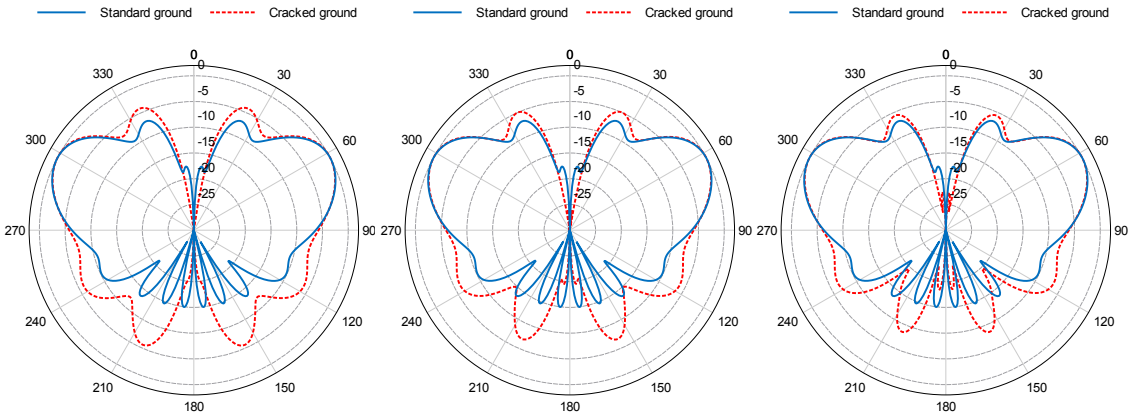

(a) (b) (c)

Figure 5.4: Radiation pattern when $d = 0.5\lambda$, $\phi = 360°$ and (a) $w = 0.1\lambda$ (b) $w = 0.05\lambda$ (c) $w = 0.01\lambda$.

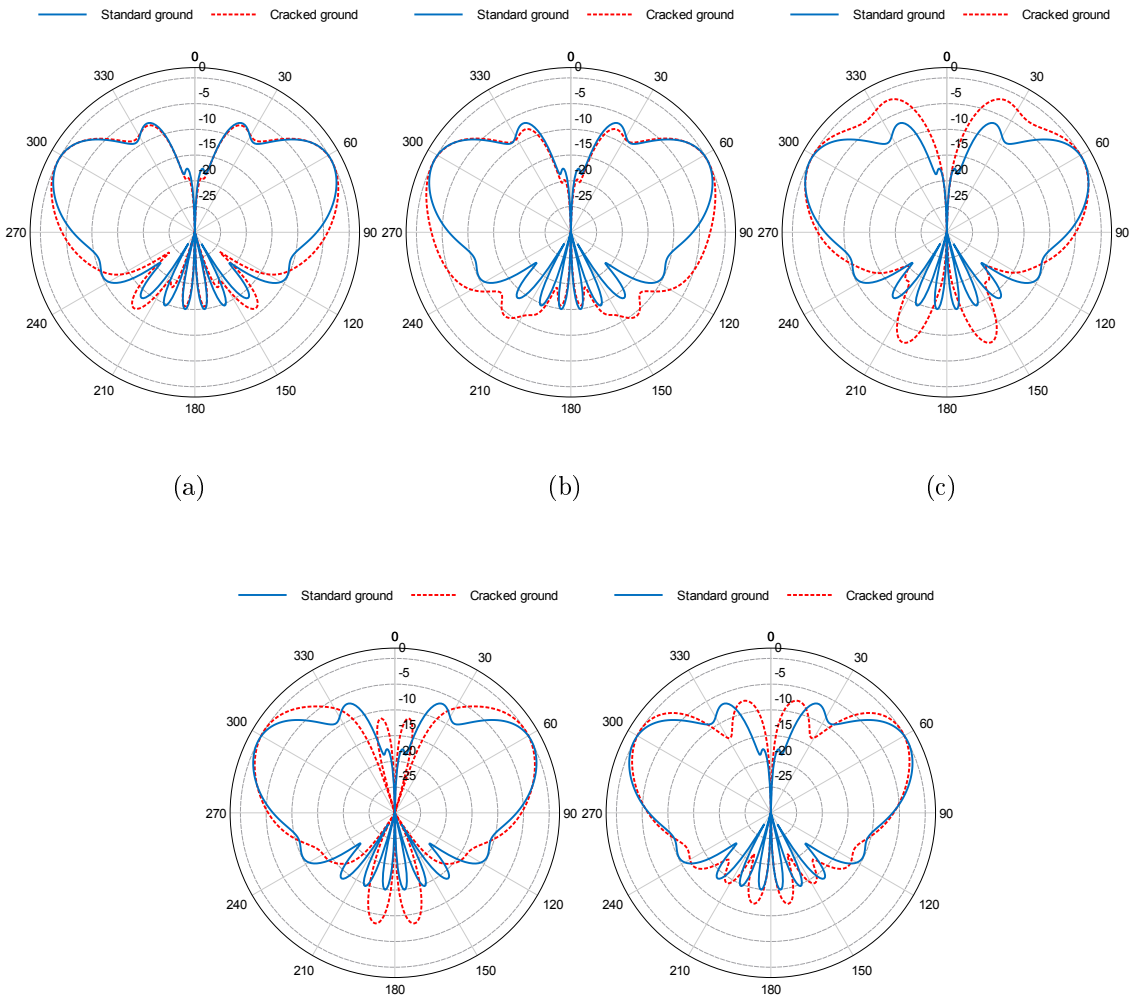

Figure 5.5: Radiation pattern when $w = 0.05\lambda$, $\phi = 360°$ and (a) $d = 0.05\lambda$ (b) $d = 0.25\lambda$ (c) $d = 0.75\lambda$ (d) $d = 1.25\lambda$ (e) $d = 1.75\lambda$.

dual of its complement antenna, i.e., the annular ring antenna. A small annular ring is in turn the dual of a short electric dipole. Thus, one could say that the radiation pattern of a small annular crack is analogous to the radiation pattern of a small dipole; therefore, when it interferes with the radiation of a quarter-wave monopole, the pattern in the upper hemisphere is not distorted much.

As the crack distance from the antenna increases, the pattern in some angular sections in the upper hemisphere changes (Fig. 5.5c). This is because as the crack distance from the antenna increases, there are more variations in the interference between the waves radiated by different portions of the cracks. These variations change the monopole pattern. By further increasing the distance, the distortion in the pattern becomes again less pronounced since the crack gets too far from the antenna and the current density impeded by the crack is weak. In all the cases, pattern distortion close to horizon is less than 2 dB.

Fig. 5.6 shows the VSWR versus the crack distance from the antenna for $w = 0.05\lambda$ and $\phi = 360°$. The source impedance is chosen for maximum power transfer (VSWR of 1:1) when no crack is introduced. Due to the near field interactions between the antenna and crack, the antenna impedance changes significantly when the crack occurs close to the antenna, especially the imaginary part. When the crack is introduced at $d = 0.05\lambda$, the reactance changes form +j18 to -j113. As the crack distances increase, the change in the impedance becomes less and less. As can be seen, at distances greater than $d = 0.2\lambda$, the VSWR is better than 2:1 and hence the impact of the crack on the antenna input impedance can be considered insignificant for most antenna applications.

Note that the introduction of cracks leads to increased radiation in the lower hemisphere due to radiation by the crack. Increasing the arc length or gap width results in an increase of the radiation into the lower hemisphere. However, this increased radiation in the lower hemisphere does not happen when cracks occur in

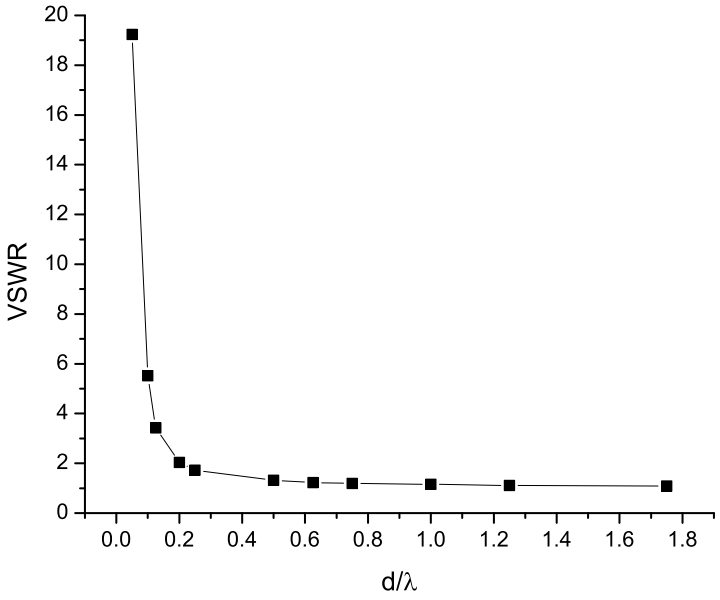

Figure 5.6: VSWR versus distance of the crack from the antenna when $w = 0.05\lambda$ and $\phi = 360°$.

the fuselage since the discontinuity is backed with the fuselage.

Fig. 5.8 shows the normalized gain pattern of a quarter-wave monopole antenna operating at 30 MHz mounted on the geometry shown in Fig. 5.7. As can be seen, the pattern is not distorted in the lower hemisphere as well as the upper hemisphere. A hollow model of the airframe is used. No details inside the airframe are modelled.

Such cracks and other apertures such as windows may permit coupling into the

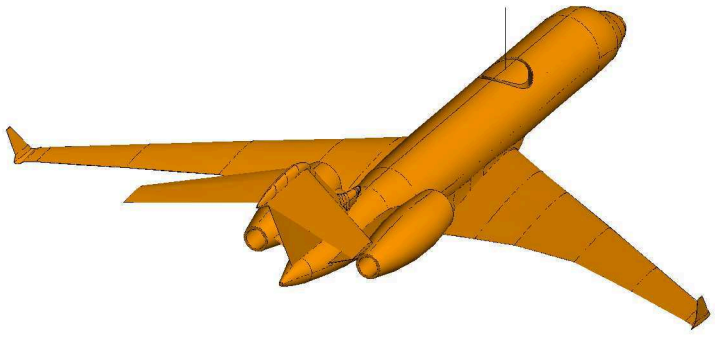

Figure 5.7: A notional crack introduced into the 1-mm thick airframe skin.

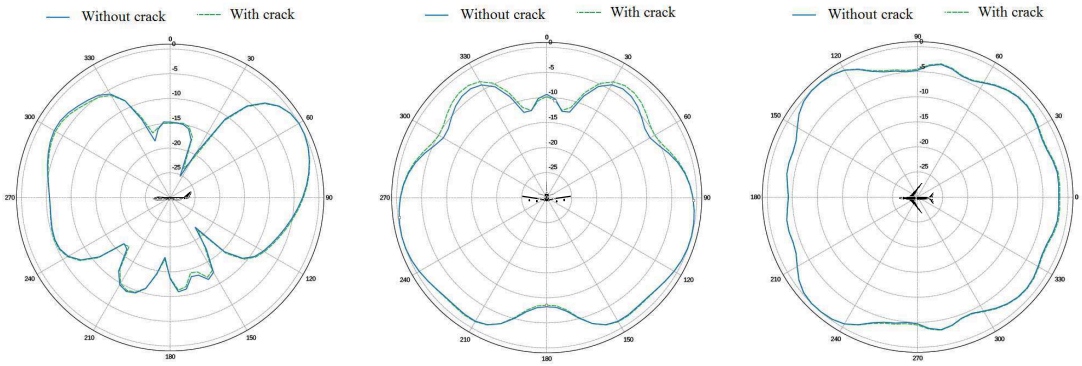

(a) (b) (c)

Figure 5.8: Radiation pattern of the model shown in Fig. 5.7 compared to the radiation pattern of the original model at 30 MHz, in (a) pitch plane (b) roll plane (c) yaw plane.

interior of the fuselage with an appropriate modification in the antenna impedance. It is not easy to examine the effect since the apertures and a reasonable presentation of the interior need to be included the model.

Chapter 6

Conclusions

In this thesis, the radiation of antennas on carbon-fibre composite aircraft was studied. The airframe scattering mechanism was analyzed and the impact of some geometry modifications on the antenna radiation was studied. The utility of the leading numerical techniques suitable for analysis of aircraft antennas at VHF and UHF frequencies was studied and benchmark data on the computational resources required was provided. The impact of cracks, seams and panel joints on the radiation of the antenna was also studied.

The study conducted in Chapter 2 can be used to devise simplified models of the aircraft geometry to calculate a desired antenna characteristic at a desired frequency within the required accuracy. The analysis was performed for a monopole antenna mounted on the fuselage. A monopole antenna was chosen since it simulates the most common type of antenna used on aircraft, i.e. blade antenna. However, the approach adopted can be applied to other types of antennas as well.

It was seen that scattering from all parts of the aircraft geometry does not have a crucial role in the formation of the radiation pattern in a particular plane. Moreover, the electrical size and distance of different aircraft parts changes at different frequencies and hence the contribution of the aircraft parts to the formation of the

radiation pattern varies with frequency. Thus, depending on the frequency and the plane in which the radiation pattern is of interest, simplified models of the aircraft can be designed and be used to validly obtain the radiation pattern.

It was also seen that at VHF and UHF frequencies, including only a wavelength of the airframe either side of the antenna is sufficient for calculation of the input impedance within reasonable accuracy. Such a simplified problem can be solved within seconds and can lead to great savings of the required computational resources specially at high frequencies where the airframe is hundreds times longer than 1λ.

In Chapter 3, the utility of the numerical techniques, MLFMM, PO and UTD, for aircraft antenna analyses was examined. The impact of the mesh size, the integral equation formulation and the choice of the pre-conditioner on the memory consumption and speed of the MLFMM were numerically studied. It was seen that a mesh with $\lambda/5$ triangle edge length is sufficiently fine for accurate calculation of both radiation pattern and input impedance and an empirical formula to estimate the number of unknowns for a given triangle edge length was presented. It was also seen that employing the CFIE formulation improves the convergence of the MLFMM iterative solution. At high frequencies, this leads to great reduction in the overall CPU-time needed for the analysis. The choice of the pre-conditioner also impacts the MLFMM convergence. In Feko, the Super-LU pre-conditioner leads to better convergence than the SPAI conditioner, but uses more memory. Thus, the Super-LU pre-conditioner can be used when fast convergence is desired and the SPAI pre-conditioner can be used at frequencies where the memory limit is reached with the Super-LU pre-conditioner, to increase the MLFMM problem size limit at the cost of slower convergence and longer simulation run.

PO was used to calculate the antenna radiation pattern at different frequencies. It was seen that at high frequencies, PO can be used to obtain a reasonable approximation of the radiation pattern at a significantly reduced cost compared to the

MLFMM. PO is, therefore, a suitable candidate for radiation pattern analysis at frequencies where the computational limits are reached with MLFMM. PO is not suitable for impedance calculations.

The validity of UTD for radiation pattern and coupling calculations when the fuselage is electrically large was examined through comparison with the MLFMM. Using UTD, the roll plane radiation pattern of a quarter-wave monopole mounted forward of the wings could be accurately calculated at 300 MHz. The mutual coupling between two short monopoles mounted on the fuselage was also calculated at 350 MHz ($ka = 10$) using UTD. The UTD results were in very good agreement with the MLFMM results for different relative positions of the two antennas. An extension of the Friis formula for calculating coupling was also proposed. The formula was deducted from the UTD solution and its validity for coupling calculations when the antennas are in each other's far fields was verified.

In Chapter 4, the impact of metal-composite junctions on the antenna performance was studied. It was shown that the distortion in the current density, caused by the change in the conductivity from to 10^7 to 10^4, is too slight to have any visible impact on the antenna radiation, even when the antenna is electrically close to the junction. The antenna input impedance can change slightly, only when the antenna is placed very close to the junction.

In Chapter 5, the effect of discontinuities caused by cracks and seams on the antenna radiation was examined. It can be concluded that the introduction of cracks might cause distortion in the antenna pattern. This distortion might not be tolerable depending on the application. Cracks at intermediate distances (about 0.75λ) from the antenna have the most significant impact on the radiation pattern in the upper hemisphere. At larger distances from the antenna the current density that is obstructed by the crack is weak and the crack radiation does not disturb the antenna radiation much. When the crack is close to the antenna, there is not much variation

in the interference between waves radiated by the antenna and different portions of the crack. Moreover, an asymmetrical crack causes asymmetry in the pattern.

It was seen that cracks can only slightly change the radiation pattern of a monopole antenna around the horizon, so they do not impact the performance of the blade antennas used for communication, navigation and identification applications where the antenna radiation around the horizon is of importance.

The impact of the cracks on the antenna input impedance depends on the distance of the crack from the antenna. The input impedance of the antenna might be altered considerably if cracks occur at locations very close to the antenna, so care must be taken to prevent or address this problem to maintain the intended antenna performance. At distances greater than $d = 0.2\lambda$, the impact of the crack on the antenna input impedance can be considered insignificant for most antenna applications.

In the future, scaled model measurements can be performed to validate the simulation results presented in this thesis. The easiest case to begin with will be the monopole antenna on a half-CFC half-aluminum ground plane studied in Chapter 4. Note that using scaled models, CFC panels cannot be used since, according to the similitude theorem, they need to be modelled by a conductivity greater than 10^4S/m, i.e. 10^4S/m divided by the similitude factor.

Moreover, the CAD model of the aircraft provided for this study was perfectly conducting and the apertures in the airframe were not modelled. The current density on the airframe when apertures are included would be different from the current density on a perfectly conducting model of the airframe. It will be worthwhile to investigate the antenna radiation when these apertures, specifically the windshields, are included in the model. The current density on the nose would be different when windshields are taken into account. The radiation pattern of the antenna in the pitch plane (where the nose is influential) may hence be different from what that was presented in this thesis, especially at low frequencies.

A model of the aircraft including the apertures will also be useful for studying coupling through the airframe. Radiation of an antenna outside the airframe may enter the inside of the airframe through the apertures and couple to the Line-replaceable Unit (LRU) of another system causing electromagnetic interference. The radiation from the units inside the airframe can also pass through the apertures and become incident on the antenna of another system impacting the performance of the antenna.

Bibliography

[1] M. Niu, *Composite airframe structures: practical design information and data.* Adaso Adastra Engineering Center, 1993.

[2] J. Kim and W. Burnside, "Simulation and analysis of antennas radiating in a complex environment," *IEEE Trans. Antennas and Propagat.*, vol. 34, no. 4, pp. 554–562, 1986.

[3] D. McNamara, C. Pistorius, and J. Malherbe, *Introduction to the Uniform Geometrical theory of diffraction.* Artech House, 1990.

[4] P. Pathak and N. Wang, "Ray analysis of mutual coupling between antennas on a convex surface," *IEEE Trans. Antennas Propagat.*, vol. 29, no. 6, pp. 911–922, 1981.

[5] R. Burberry, *VHF and UHF antennas.* Peter Peregrinus Ltd, 1992.

[6] G. Weinstock, "Electromagnetic integration of composite structure in aircraft," in *NATO Advisory Group for Aerospace Research and Development, Avionics Panel, Conference*, no. 283. DTIC Document, 1980.

[7] J. Allen, A. Adams, W. Gajda, and W. Walker, "Electromagnetic properties and effects of advanced composite materials: Measurement and modeling," RADC-TR-78-156, Phase Report, Tech. Rep., 1978.

[8] W. Gajda, "A fundamental study of the electromagnetic properties of advanced composite materials," DTIC Document, Tech. Rep., 1978.

[9] C. Blake and J. Corbin, "Electrical/electromagnetic concerns associated with advanced composite materials in aerospace systems," *AGARD Electromagnetic Effects of (Carbon) Composite Mater. Upon Avionics Systems 8 p(SEE N 81-16144 07-24)*, 1980.

[10] D. Brewster, "Theoretical calculation of rf properties of carbon fibre laminates," *AGARD Electromagnetic Effects of(Carbon) Composite Mater. Upon Avionics Systems 16 p(SEE N 81-16144 07-24)*, 1980.

[11] C. Balanis and D. DeCarlo, "Monopole antenna patterns on finite size composite ground planes," *IEEE Trans. Antennas Propagat.*, vol. 30, no. 4, pp. 764–768, 1982.

[12] D. Strawe, "Electromagnetic shielding characteristics of advanced composites," in *AGARD Conference Proceedings*, vol. 283. DTIC Document, 1980.

[13] T. Macnamara, *Introduction to antenna placement and installation*. Wiley, 2010.

[14] R. Sun and C. Reddy, "Benchmark study on computational resources for numerical methods in electromagnetics," in *IEEE International Symposium on Antennas and Propagation*. IEEE, 2008, pp. 1–4.

[15] M. Heckler and A. Dreher, "Analysis of monopoles installed on airframes," in *IEEE Antennas and Propagation Society International Symposium Proceedings*, vol. 2, 2005, pp. 280–283.

[16] R. Coifman, V. Rokhlin, and S. Wandzura, "The fast multipole method for the wave equation: A pedestrian prescription," *Antennas and Propagation Magazine, IEEE*, vol. 35, no. 3, pp. 7–12, 1993.

[17] M. Nieto-Vesperinas, *Scattering and diffraction in physical optics*. New York, 1991.

[18] *FEKO user manual, Suite 6.1*, EM Software and Systems-S.A. (Pty) Ltd, July 2011.

[19] O. Givati and A. Fourie, "Radiation patterns of antennas mounted on a modified mirage aircraft," in *Antennas and Propagation Society International Symposium, 1994. AP-S. Digest*, vol. 2. IEEE, 1994, pp. 1158–1161.

[20] Bombardier Inc. 800 René-Lévesque Boulevard West, Montréal, QC, Canada H3B 1Y8. [Online]. Available: http://www.bombardier.com

[21] P. Kazerani and R. Paknys, "Analysis of monopole antennas mounted on the fuselage of carbon-fibre composite aircraft," in *AERO 11 58th Aeronautics Conference and AGM, Canadian Aeronautics and Space Institute*, Montreal, QC, 2011, pp. 26–28.

[22] B. Piper and M. Bialkowski, "Electromagnetic modeling of conformal wideband and multi-band patch antennas by bridging a solid-object modeler with mom software," *Antennas and Propagation Magazine, IEEE*, vol. 46, no. 5, pp. 42–52, 2004.

[23] [Online]. Available: http://www.solidworks.com/

[24] C. Balanis, *Antenna theory: analysis and design*. J. Wiley, New York, 1982.

[25] A. Rudge, *The handbook of antenna design*. Peter Peregrinus Ltd, 1983, vol. 2, ch. 17, VHF and UHF antennas.

[26] E. Miller, "A selective survey of computational electromagnetics," *IEEE Trans. Antennas Propagat.*, vol. 36, no. 9, pp. 1281–1305, 1988.

[27] R. Hodges and Y. Rahmat-Samii, "An iterative current-based hybrid method for complex structures," *IEEE Trans. Antennas Propagat.*, vol. 45, no. 2, pp. 265–276, 1997.

[28] S. Davidson and G. Thiele, "A hybrid method of moments-gtd technique for computing electromagnetic coupling between two monopole antennas on a large cylindrical surface," *IEEE Transactions on Electromagnetic Compatibility*, no. 2, pp. 90–97, 1984.

[29] A. Barka and P. Caudrillier, "Domain decomposition method based on generalized scattering matrix for installed performance of antennas on aircraft," *IEEE Trans. Antennas Propagat.*, vol. 55, no. 6, pp. 1833–1842, 2007.

[30] W. Stutzman and G. Thiele, *Antenna theory and design*. J. Wiley, 1998, vol. 320.

[31] J. Song and W. Chew, "Multilevel fast-multipole algorithm for solving combined field integral equations of electromagnetic scattering," *Microwave and Optical Technology Letters*, vol. 10, no. 1, pp. 14–19, 1995.

[32] A. Poggio and E. Miller, "Integral equation solutions of three-dimensional scattering problems," *Computer techniques for electromagnetics.(A 73-42839 22-07) Oxford and New York, Pergamon Press*, pp. 159–264, 1973.

[33] R. Johnson and H. Jasik, *Antenna engineering handbook*. McGraw-Hill, 1984, vol. 1.

[34] S. Rao, D. Wilton, and A. Glisson, "Electromagnetic scattering by surfaces of arbitrary shape," *IEEE Trans. Antennas Propagat.*, vol. 30, no. 3, pp. 409–418, 1982.

[35] P. Foster, "The region of application in gtd/utd," in *Computation in Electromagnetics, Third International Conference on (Conf. Publ. No. 420)*. IET, 1996, pp. 382–386.

[36] P. Pathak, N. Wang, W. Burnside, and R. Kouyoumjian, "A uniform gtd solution for the radiation from sources on a convex surface," *IEEE Trans. Antennas Propagat.*, vol. 29, no. 4, pp. 609–622, 1981.

[37] J. Richmond, "A reaction theorem and its application to antenna impedance calculations," *IRE Transactions on Antennas and Propagation*, vol. 9, no. 6, pp. 515–520, 1961.

[38] N. Logan, *General research in diffraction theory*. Lockheed Missiles and Space Division, Lockheed Aircraft Corporation;[available from the Armed Services Technical Information Agency, Washington], 1959, vol. 2.

[39] H. Booker, "Slot aerials and their relation to complementary wire aerials (babinet's principle)," *Electrical Engineers-Part IIIA: Radiolocation, Journal of the Institution of*, vol. 93, no. 4, pp. 620–626, 1946.